This document was prepared in conjunction with work accomplished under Contract No. DE-AC09-76SR00001 with the U.S. Department of Energy.

DISCLAIMER

TECHNICAL DIVISION
SAVANNAH RIVER LABORATORY

DPST-83-992

ACC. NO. 120186

DISTRIBUTION:

1. M. R. BUCKNER, 773-A
2. R. M. HARBOUR, WILM
3. J. E. CONAWAY, WILM
4. J. T. GRANAGHAN, SRP, 703-A
5. A. H. PETERS, 703-A
6. J. L. WOMACK, 703-A
7. G. F. MERZ, 703-54A
8. L. HIBBARD, 703-A
9. F. BERANEK, 706-C
10. L. R. CHANDLER, 706-C
11. C. G. REYNOLDS, 706-C
12. S. MIRSHAK, SRL, 773-A
13. J. R. HILLEY, 773-A
14. S. D. HARRIS, 773-A
15. W. E. GRAVES, 773-24A
16. D. A. SHARP, 773-24A
17. P. L. AMES, 773-24A
18. N. P. BAUMANN, 773-A
19. D. S. CRAMER, 773-24A
20. J. R. CHANDLER, 773-24A
21. SRL RECORDS, 773-A, (4)

December 30, 1983

TO: M. R. BUCKNER, 773-A

FROM: J. R. CHANDLER
JRC

THIS FILE
RECORD COPY

MARK 22 REACTIVITY

INTRODUCTION

Calculations for reactivity held in control rods have underpredicted the observed Mark 22 reactivity by 100 μB to 200 μB. Reactivity predictions by charge designers have accounted for this by including large biases which change with exposure and reactor region.

The purpose of the study described here was to thoroughly investigate the methods and data used in the reactivity calculations. The goal was to identify errors and improvements and make necessary corrections.

SUMMARY

Several improvements in Mark 22 reactivity calculations have been identified and implemented. These improvements yield significantly better agreement between calculated and observed reactivity held in control. The calculated change in reactivity with increasing exposure now agrees with observed data. The large difference in absolute reactivities for stage 1 Mark 22 operation has been reduced by a factor of 3. A constant bias factor of +55 μB can be applied to account for the remaining difference

during single stage and stage 1 operation, and a constant bias factor of -50 μB can be applied to account for the remaining difference during stage 2 operation.

Thorough investigation of methods and data has failed to obtain complete agreement between calculated and observed data. The remaining difference is probably due to the following:

- o Bias exists in measurement of target and control rod ^{6}Li contents.
- o Nuclear cross section data, including recent improvements, are still not adequate.
- o Methodology of the JASON code for calculating axial burnup is inexact.

Routine application of the neutron transmission method for measuring ^{6}Li contents of standards was proposed in a previous study.[1,2] It is recommended that this proposal be implemented and current standards be remeasured. An engineered facility for routine measurement using neutron transmission could improve the accuracy of ^{6}Li measurements by a factor of 2 to 3.[1]

Investigation of input specifications normally used for GLASS Mark 22 calculations revealed inadequate nuclear data and incorrect vertical leakage[3]. Corrections for these problems have included developing improvements to SRL nuclear data and use of 40μB for vertical leakage. Mark 22 GLASS calculations should be made using improved data for ^{235}U, ^{6}Li, Al, and fission products described in this document. Mark 22 JASON calculations should use a data library based on GLASS and the new data. JASON calculations should be made using vertical leakage buckling of 40μB.

Future improvements are planned for nuclear cross section data and JASON methodology for calculating axial burnup. These improvements should eliminate deficiencies in nuclear cross section data and JASON axial burnup methodology.

DISCUSSION

GLASS Options

GLASS options were investigated to determine if the options used by SRL and SRP are adequate for Mark 22 calculations. These options include transport method, resonance method, energy group structure, geometric mesh point spacing, and subregion geometry.

GLASS calculational options nominally used when generating PARMEQ libraries for use with JASON are integral transport and CREEP resonance calculations. These options were compared against state-of-the-art Monte Carlo and RRR1DZ[4] resonance calculations. In a sample Mark 22 lattice buckling calculation integral transport results were shown to agree very closely with Monte Carlo results. The statistical error associated with the Monte Carlo calculation is 11 μB at 95% confidence. A similar comparison of results from the CREEP and RRR1DZ resonance treatments shows agreement within 10 μB, with CREEP being higher than RRR1DZ. Use of Monte Carlo and RRR1DZ will not reduce the difference between observed and calculated reactivity.

A 37 group energy structure is normally used for Mark 22 GLASS calculations. An 84 group energy structure was used in a sample problem. Results from the 37 group structure agree with results from the 84 group structure to within 1 μB.

A previous study[5] showed GLASS results for k_{eff} depend on mesh point spacing and recommended a spacing interval of 0.01 cm for Mark 22 calculations. A buckling calculation was made with 0.005 cm mesh spacing; the result agrees with a 0.01 cm mesh spacing calculation to within 1 μB.

Another GLASS option is the use of subregion to divide regions. Use of subregions provides a more detailed representation of the flux gradient because the flux is averaged in each subregion rather than over an entire region. Mark 22 GLASS calculations are normally made with coolant and moderator regions divided into 2 or 3 subregions and all other regions not subdivided. Doubling the number of moderator and coolant subregions resulted in no change in GLASS buckling results. Subdividing fuel and target regions into 4 subregions along with doubling moderator and coolant subregions also produced no buckling change.

GLASS options nominally used for Mark 22 calculations (integral transport, CREEP resonance treatment, 37 group energy structure, 0.01 cm mesh point spacing, moderator region subdivision, and no subdivision of fuel and target) are therefore sufficiently accurate. No substantial improvement can be gained by more detailed calculations. Comparison of GLASS options is summarized in Table I.

Nuclear Data

Good nuclear data are essential for accurate prediction of reactor parameters. Several sets of nuclear data are available for use with GLASS calculations. In addition newer data than that in SRL datasets are available. Evaluation of the adequacy of current data is discussed in the following paragraphs.

Nuclear data for ^{235}U in the current JOSHUA.STD.MULTIGRP dataset versions STANDARD and STD37 are based on ENDF/B-III (Evaluated Nuclear Data Files B, Version III) of 1972 with SRL modifications.[6] Nuclear data for ^{6}Li and Al are from data prior to ENDF/B-III. Comparisons with more recent data were made to evaluate the adequacy of data for Mark 22 calculations. Recent data (ENDF/B-V) for Al have a smaller epithermal neutron absorption cross section. Recent ^{235}U data have different fission and capture cross sections and ν values, leading to a higher value for η (where $= \frac{\nu\sigma_f}{\sigma_f + \sigma_\gamma}$ = number of neutrons emitted per neutron absorbed.)

At this time* SRL processing codes are not compatible with ENDF/B-V data formats. ENDF/B-IV however was processed and provides the same ^{6}Li and Al data as does ENDF/B-V. ENDF data for ^{235}U was modified between version IV and version V. The largest effect of this modification on Mark 22 calculations is in the increase in η. A modified set of ^{235}U data, called U235E4/5 was developed for temporary use with Mark 22 calculations. The modified ^{235}U data consists of pure ENDF/B-IV cross sections and modified ENDF/B-IV ν data. The ν modification was derived so thermal η of U235E4/5 is equal to thermal η of ENDF/B-V. The effects of improved nuclear data on GLASS buckling results are summarized in Table II. After update of SRL data processing codes ENDF/B-V data will be processed for use with GLASS.

Results from a previous investigation[3] into GLASS fission-product data were used in this study. As discussed in documentation[3] of that previous study, the SHIELD[7] system offers an alternative to the fission product poisoning treatment in GLASS. The SHIELD calculation is more detailed, requires more computer time, and is usually not used when generating JASON libraries. Comparison of GLASS and SHIELD fission product poisoning indicated fission product data for GLASS was inadequate. In particular the cross sections for ^{147}Pm, ^{148}Pm, and ^{148m}Pm in JOSHUA.STD were found to be incorrect and the long term fission product treatment needed improvement. The corrected ^{147}Pm, ^{148}Pm, and ^{148m}Pm cross sections were obtained from W. E. Graves and used in this study. Data for a two-lumped fission product treatment[3], accomplished using two fictitious isotopes, were also obtained from W. E. Graves and used.

*SRL has a program to update data processing codes to be compatible with ENDF/B-V formats.

Vertical Leakage

A vertical buckling of 60 μB has been traditionally used in SRP lattice and reactor calculations to account for vertical leakage. This value probably was derived from a calculation years ago assuming a bare reactor. An accurate calculation includes reflectors and observed Mark 22 flux shape. The result from such a calculation[3] for vertical leakage is 40 μB. The 40 μB value was used in GLASS and JASON calculations for this study.

SE Measured Buckling

Several Mark 22 lattice buckling measurements[8] were made in the Subcritical Experiment (SE) in the early 1970's. The measurement results can be compared with GLASS results to get an indication of the accuracy of the nuclear data and GLASS methods (Table III). The calculated buckling is from 25 μB to 55 μB low. An uncertainty of this comparison is the target ^{6}Li content of the measured assemblies (see Appendix A). The buckling differences between calculations and SE measurements are consistent with differences between calculated and observed start-of-cycle buckling in control. This indicates an error of about 50 μB in the calculation of reactivity for an unirradiated Mark 22 lattice.

JASON Code Changes

Two coding errors in JASON, one in the GRIMHX module and one in the XGRIM module, were discovered in this study. Both errors affect calculations that flatten to average fuel powers. The GRIMHX error occurs when determining average powers of clusters with vacant positions. This error leads to incorrect gang power when vacant positions exist within the gang, such as gang 3 in cycles C-2 and C-3. Since gang power influences reactivity held in control, this coding error adversely affects the radial buckling shape calculated by JASON for charge designs with vacancies in control regions. The XGRIM coding error occurs in subroutine GRASP where a flag is set according to the flattening option chosen. The error causes JASON to flatten power using maximum fuel powers when the user specifies average fuel powers. The average fuel power option is nominally not used by RTD charge designers, so their past JASON results are probably not affected. A corrected version of JASON was used for calculations in this study. The corrected version of JASON will be made the production version using the procedures for such a change.

Summary Of JASON Input

JASON presents the user several options. Particularly important are options concerning power flattening, control zone

structure, and axial exposure weighting. In future Mark 22 charge design it is recommended that:

- o Patch structure be used for control zone breakup.
- o JASON flattening option No. 4 (cluster power is maximum assembly power, control zone power is average cluster power) be used.
- o No radial power shape be specified
- o No axial weighting be used.

Further discussion of these JASON options is contained in Appendix B.

Vertical leakage is specified in the INPUT.REX.JASON.SPECS record. The record in the JOSHUA.STD dataset contains a value of 60 μB. For Mark 22 calculations an INPUT.REX.JASON.SPECS record should be created in the user's data set with value 40 μB.

Three different JASON libraries were utilized during this study. Results reported here were calculated with JASON using a new library[9] with all nuclear data improvements discussed earlier. This library will be placed in the JOSHUA.STD dataset for future use with Mark 22 calculations.

Summary Of JASON Calculations

Present JASON reactivity calculations give better agreement with observed reactivity in control than past results (Figure 1). Past Mark 22 JASON calculations have greatly underpredicted buckling held in control necessitating large biases be added to calculated results. Biases, obtained from analysis of Mark 22 operating data, have in the past varied between reactor gangs and varied with exposure.

Results from current reactivity calculations were compared with observed data for Mark 22 cycles C-2.1, C-2.2, C-3.1, K-6.1, and K-6.2. Present calculated results are about 100 μB higher than past calculated results though absolute agreement between calculated and observed data is still not attained. Present results (Figure 1) show the change in reactivity as a function of subcycle exposure agrees with observed data. A constant bias factor can be applied in each subcycle to account for the absolute difference. In fact for all calculations other than final charge predictions a +55 μB bias can be used for all gangs in stage 1 and a -50 μB bias for all gangs in stage 2. Application of these bias factors gives excellent agreement between calculated and observed

reactor-averaged reactivity (Figures 2-4) and acceptably good agreement on a gang-wise basis.

Discussion of Remaining Difference

Thorough investigation of methods and data failed to obtain complete agreement between calculated and observed data. The reactivity difference for stage 1 operation is not the same as the reactivity difference for stage 2. The stage 1 and 2 differences will be discussed separately.

The remaining difference for stage 1 or single stage calculations is probably due to a combination of the following:

- o Bias exists in measurement of target and control rod ^{6}Li contents
- o Nuclear cross section data, including recent improvements, are still not adequate.

Much of the difference is probably due to uncertainty in ^{6}Li content of fabricated targets. Standards for the nuclear test gauge (NTG) have been calibrated[1,2] with an estimated absolute accuracy of $\pm 3\%$. An error in the standards will bias all NTG measurements. A 3% bias in typical inner target contents will produce 15 μB error for gang III targets and 25 μB error for gangs I and II. A 3% bias in typical outer targets will produce 20 μB error in gang III and 25 μB error for gangs I and II. Thus a 3% uncertainty in ^{6}Li target contents leads to about 45 μB uncertainity in reactor averaged reactivity held-in-control.

Bias may also exist in NTG measurements of ^{6}Li in control rods. The contents of control rod standards were determined in the early 1970's with destructive analysis and have not been determined with the neutron transmission method. The destructive analysis technique has a history of poor accuracy and comparison[1] of neutron transmission and destructive analysis results for Mark 22 inner targets show differences of 13% to 18%. A bias in control rod contents would have an impact on the difference between observed and calculated reactivity held in control.

The best available nuclear data (ENDF/B-V) for ^{235}U cannot be processed into a form suitable for GLASS because SRL cross section processing codes are not compatible with new formats universally used for data storage. Modification of the processing codes is planned for the future. In lieu of ENDF/B-V ^{235}U data, data from ENDF/B-IV was modified and used. It cannot be determined how much of the remaining discrepancy between calculated and observed reactivity is due to nuclear data. This remains an area for possible improvements.

The stage 2 difference between observed and calculated reactivity held in control is probably due to the items listed for stage 1 and also due to JASON methodology for calculating axial burnup. The methodology used in JASON to calculate axial burnup effects is an approximation. Exposures for different axial regions are averaged by JASON to determine assembly exposure. If desired JASON weights the assembly averages with the axial power profile specified by the user. Generally JASON assembly exposure does not accurately reflect differences between flux in the central region and flux near the top and bottom of the assembly. When no axial weighting is used JASON overpredicts start-of-stage 2 reactivity held in control. When observed axial power is used to weight assembly exposures buckling in control is close at stage 2 start but becomes increasingly incorrect as exposure increases.

Three dimensional methodology is being developed to calculate reactivity held in control. The new methodology should provide multistage calculations with no relative bias between stages.

REFERENCES

1. N. P. Baumann, "Verification of NTG Standards by Thermal Neutron Transmission," DPST-81-497, July 23, 1981.

2. J. L. Hansen, "Thermal Neutron Transmission For Assaying NTG ^{6}Li Standards," RTM-300-85, July 17, 1981.

3. W. E. Graves, "Productivity Of the Mark 22 Charge," DPST-83-627, August 5, 1983 (Secret).

4. D. R. Finch, "Comparison of GLASS-RRR1D Lattice Calculations To Other Benchmark Quality Calculations," DPST-79-478, September 7, 1979.

5. A. O. Smetana, "GLASS Conversion To the FORTRAN Q Compiler," DPST-82-209, January 6, 1982.

6. F. J. McCrosson and D. A. Sharp, "Evaluation of ^{235}U and ^{238}U Cross Sections," DPST-72-340, May 9, 1972 (Secret).

7. D. R. Finch, J. R. Chandler, and J. P. Church, "The SHIELD System," Trans. Amer. Nuclear Society, 33, 413 (1979).

8. J. R. Smotrel, "Measured Physics Characteristics of the Mark 22 Lattice," DP-1326, August, 1974 (Secret).

9. J. R. Chandler, "Mark 22 JASON Charge Design Library," to be issued.

10. B. R. Adams and F. D. Benton, "K-1 Mark 22 Lithium Targets," RTM-4169, March 13, 1978.

11. "Works Technical Monthly Report," DPST-74-1-7, July 1974 (Secret).

12. J. L. Hansen, "Low-K NTG-Mark 22 AI Tests," memorandum, March 18, 1981.

13. J. L. Hansen, "Low-K NTG Calibration-April 1981," RTR-1953, Addendum 1, May 26, 1981.

14. J. L. Hansen, "Low-K NTG Fuel Calibration-1979-1981," RTR-1953, February 23, 1981.

15. P. L. Ames, "Technical Details-Control Rod Production Code," DPST-82-384, June 22, 1982.

16. P. L. Ames and W. E. Graves, "Detailed Mark 22 Reactivity Calculations," DPST-83-464, June 8, 1983.

TABLE I

BUCKLING COMPARISON OF GLASS OPTIONS

Nominal Input	Change	ΔB_m^2, μB
Integral Transport	Monte Carlo	2
CREEP	RRR1DZ	-8
37 energy groups	84 energy groups	<1
0.01 cm mesh spacing	0.005 cm mesh spacing	<1
3 moderator subregions and 2 coolant subregions	6 moderator subregions and 4 coolant subregions	<1
No target subregions	2 target subregions	<1
3 moderator, 2 coolant, 1 outer target, 1 inner target, 1 outer fuel, and 1 inner fuel subregions	6 moderator, 4 coolant, 2 outer target, 2 inner target, 2 outer fuel, 2 inner fuel subregions	<1

TABLE II

BUCKLING CHANGES FROM IMPROVEMENTS

Improvement	$\Delta B^2 m, \mu B$
^{6}Li Cross Sections	5-10
^{27}Al Cross Sections	15-20
^{235}U Cross Sections	65-75
Vertical Leakage	20

TABLE III

MEASURED/CALCULATED BUCKLING COMPARISON

^{6}Li TARGETS, gm/ft[a]		BUCKLING, μB	
INNER	OUTER	SE MEASUREMENT	GLASS CALCULATION
3.339	1.223	262	233
3.339	1.129	374	339
3.339	0.923	608	581
2.946	1.223	348	318
2.946	1.129	473	424
2.946	0.923	702	667
2.641	1.129	550	497
2.641	0.923	796	741

[a] Corrections to NTG measurements have been applied to account for calibration errors.

FIGURE 1

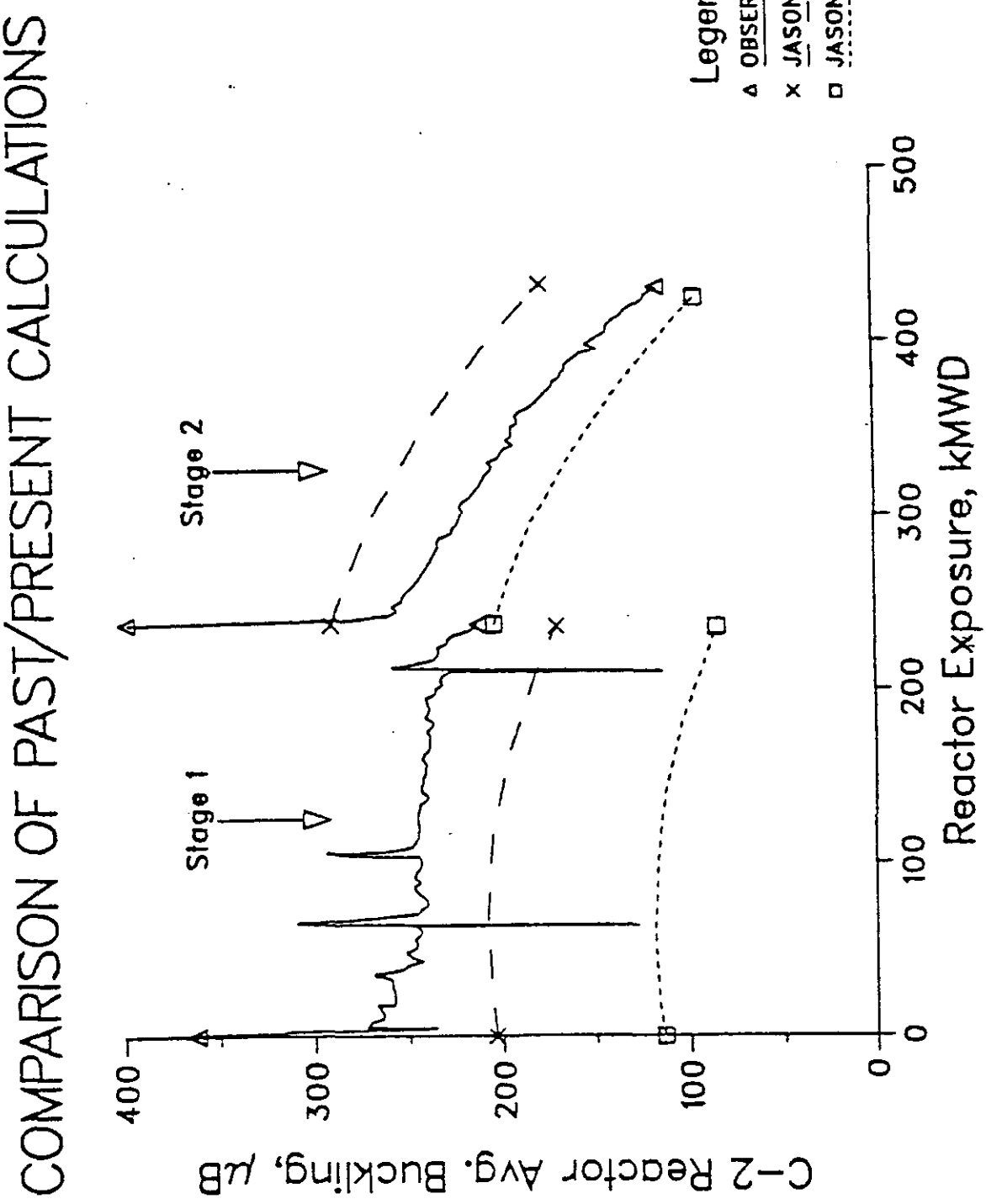
COMPARISON OF PAST/PRESENT CALCULATIONS
Legend
OBSERVED
JASON-PRESENT
JASON-OLD
Stage 1
Stage 2
C-2 Reactor Avg. Buckling, μB
Reactor Exposure, kMWD
400
300
200
100
0
0
100
200
300
400
500

FIGURE 2

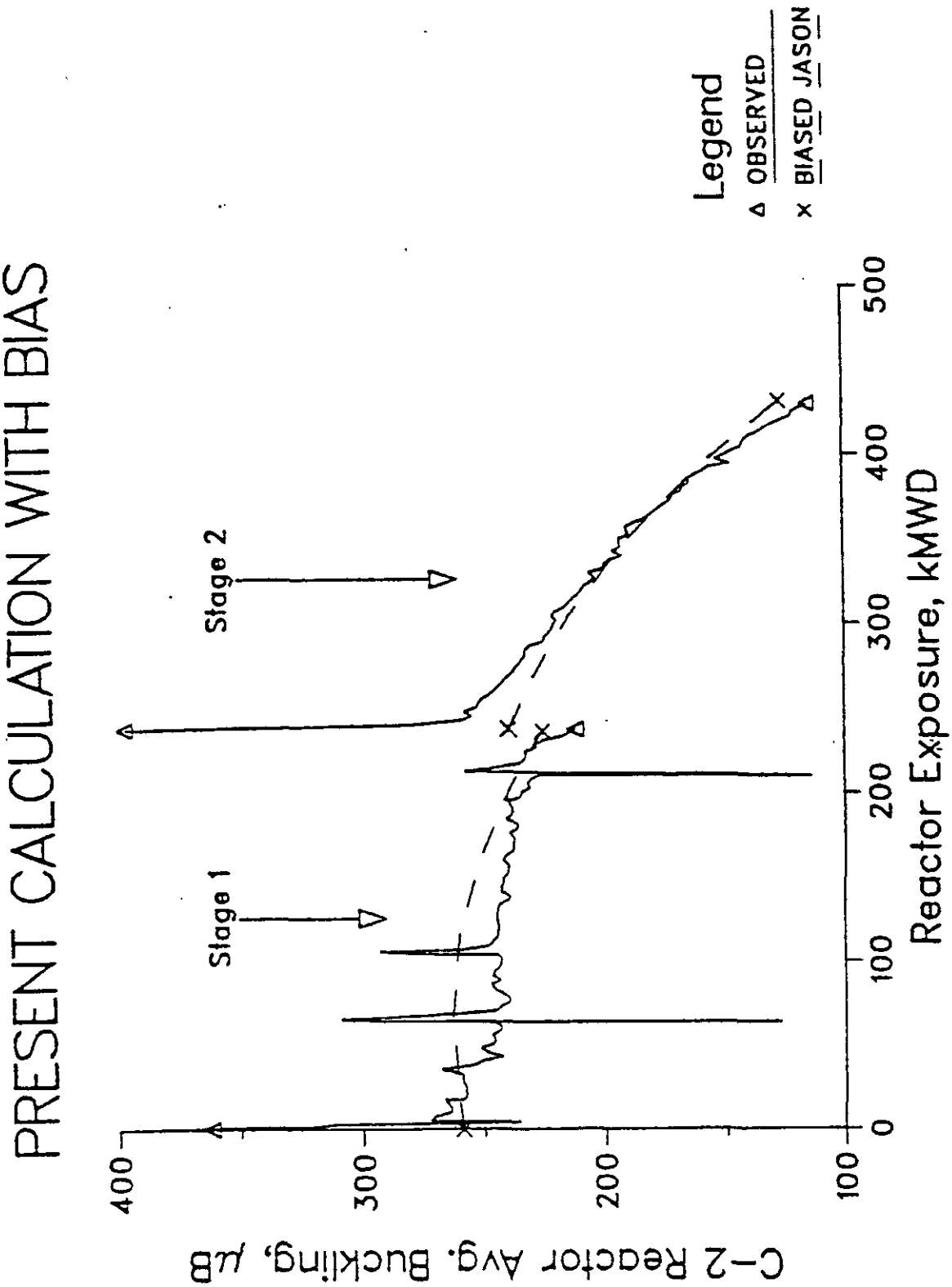
PRESENT CALCULATION WITH BIAS
Legend
OBSERVED
BIASED JASON
Stage 1
Stage 2
C-2 Reactor Avg. Buckling, μB
Reactor Exposure, kMWD
100
200
300
400
0
100
200
300
400
500

FIGURE 3

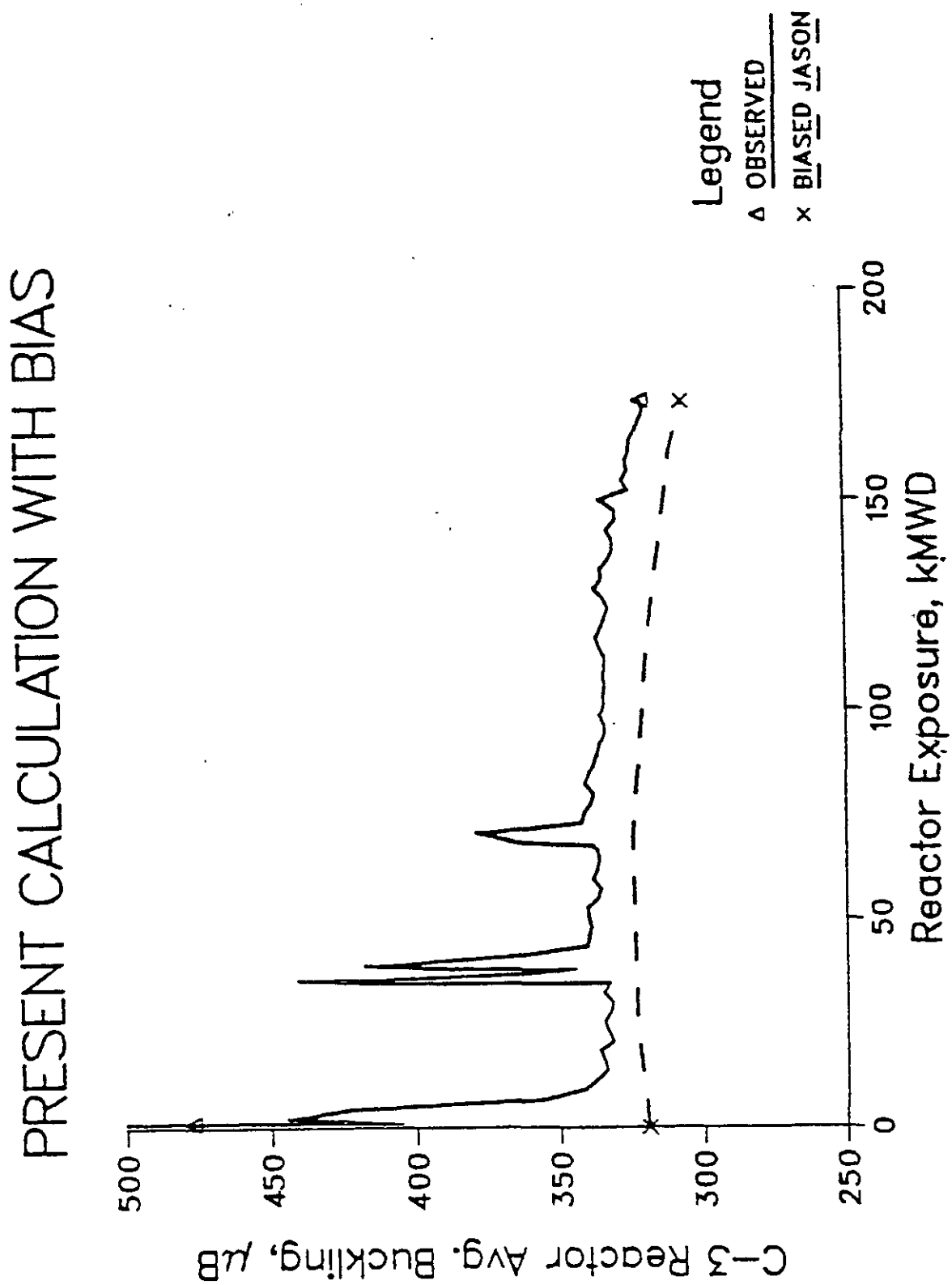
PRESENT CALCULATION WITH BIAS
Legend
Δ OBSERVED
× BIASED JASON
C-3 Reactor Avg. Buckling, μB
500
450
400
350
300
250
0
50
100
150
200
Reactor Exposure, kMWD

FIGURE 4

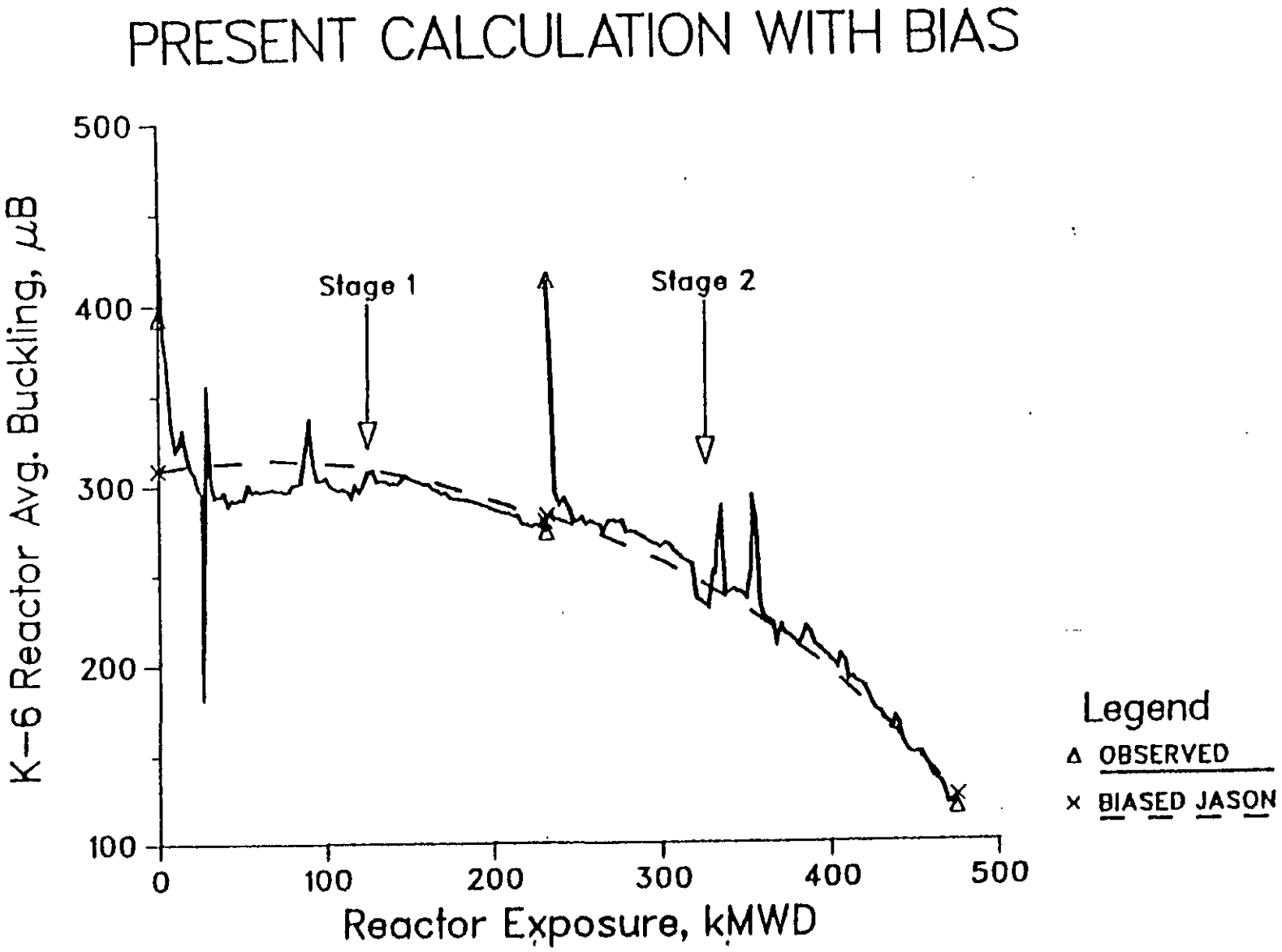
PRESENT CALCULATION WITH BIAS
K-6 Reactor Avg. Buckling, μB
500
400
300
200
100
0
100
200
300
400
500
Reactor Exposure, kMWD
Stage 1
Stage 2
Legend
Δ OBSERVED
× BIASED JASON

Appendix A - History of Mark 22 NTG Standards

Determination of fuel and target content is made using the nuclear test gauge (NTG). Prior to July of 1979 the NTG operated in a mode referred to as "full core." In July of 1979 it was converted to a low-k_{eff} facility with smaller core size. The accuracy of the NTG for determination of ^{6}Li content is limited by the method used for assaying ^{6}Li contents in calibration standards. Prior to conversion to a low-k_{eff} NTG, destructive analysis was accepted as being representative of tube contents. In the destructive analysis approach ring segments are taken from the ends of the standard or from a companion tube. The lengths of the segments are carefully measured and the segments are dissolved. The total lithium content and lithium isotopic ratios are determined by various analytical procedures. The destructive analysis technique had a history of poor accuracy. After conversion to the low-k_{eff} NTG, ^{6}Li standards were assayed using nondestructive thermal neutron transmission measurements.[1,2]

At least three sets of standards have been used with the NTG for Mark 22 assemblies. The first set was used during fabrication of the first Mark 22 charge, K-5 (1972), and the second charge, K-9 (1974). During production testing of the K-9 second subcycle inner targets, a difference between the calibration curves for the K-9.1 and K-9.2 subcycle inner targets was recognized.[10,11] The difference was caused by an error made in 1971 in ^{6}Li chemical analysis of the target standards. The error resulted from an incorrect dilution of laboratory standard lithium solution. To correct for this error NTG measurements of inner and outer target ^{6}Li content should be increased 7% if the targets were fabricated before the K-9.2 subcycle of 1974.

Another set of standards was used during fabrication of the third Mark 22 charge, K-4(1978). This set provided the same[12] calibration as the set for K-9, after correcting for the error in K-9.1 target measurements. A third set of standards was made for conversion to the low-k_{eff} NTG. The standards for the low-k_{eff} NTG have been analyzed using thermal neutron transmission[1,2] with an absolute accuracy of about $\pm$ 3%. The K-4 charge was not irradiated until after conversion to the low-k_{eff} NTG so some K-4 targets were rechecked in the low-k_{eff} NTG. The low-k_{eff} NTG results for K-4 inner targets are significantly different than full core NTG results due to the new standards calibration. Inner targets originally thought to have 2.20 gm/ft ^{6}Li were found to have 2.60 gm/ft. Inner targets originally thought to have 2.89 gm/ft ^{6}Li were found to have 3.26 gm/ft. Using this data a linear equation can be derived for the factor to be used when correcting full core NTG measurements of inner targets.

Correction factor (%) = 35.42 - 7.826 * ^{6}Li content measured in full core NTG

Full core NTG results for outer targets match low-k_{eff} NTG results. Results[13] from fuel tube measurements however differ. The differences are attributed[14] to the NTG calibration technique, destructive analysis sampling methods, interpretation of data, and uncertainties in the chemical analysis. The average ^{235}U content of inner fuel tubes were 3.59% lower and the average ^{235}U contents of outer fuel tubes 1.2% lower when tested with the low-k_{eff} NTG than with the full core NTG.

All correction factors discussed in this section were applied to documented[8] SE contents (Table A-1) for the GLASS calculations. A significant effort was given to researching the NTG history and all pertinent facts are believed to have been uncovered. However use of NTG ^{6}Li measurements made prior to 1981 should include large uncertainty.

TABLE A-1

SE MARK 22 ASSEMBLY CONTENTS

ISOTOPE	NTG MEASUREMENT, gm/ft	CORRECTED VALUE, gm/ft
^{235}U-Inner Fuel	117.8	113.6
^{235}U-Outer Fuel	131.3	129.7
^{6}Li-Inner Fuel	2.094	2.641
	2.385	2.946
	2.783	3.339
^{6}Li-Outer Fuel	0.863	0.923
	1.055	1.129
	1.143	1.223

APPENDIX B - JASON Calculations

Results

Results from JASON calculations were compared with observed data for charges C-2.1, C-2.2, C-3.1, K-6.1, and K-6.2. The comparisons show there is still an unexplained difference in reactivity held in control. Generally it is recommended that JASON calculations of Mark 22 charges be biased in each gang by +55 μB for stage 1 and -50 μB for stage 2. For special applications, such as specifying final charge design parameters, separate bias factors should be applied for each gang. These biases can be derived from Figures B-1 through B-20 or from similar data current to the charge being designed. Application of the biases above (Figures B-21 through B-40) gives excellent agreement between calculated and observed reactor-averaged bucklings and acceptable agreement on a gang-wise basis.

Observed data was obtained using the Control Rod Production (CRP) code.[15] CRP calculates reactivity held in control rods using the method and data in reference 16. Reactor-averaged buckling is based on statistical weights calculated by JASON. Observed reactivity data (Figures B-1 through B-20) show various control rod moves made during reactor operation. Spikes in observed data indicate reactor scrams. The large initial decrease in buckling held in control at startup is due to rods being withdrawn as reactor power is increased and fission product poisons build in. Curves labeled "JASON-2" are results using JASON flattening option No. 2 and "JASON-4" are results using flattening option No. 4. Curves labeled "-GANG" are results using gang control structure and specified radial power shape (Tables B-1 and B-2). Curves labeled "-PATCH" are results using patch control structure and no specified radial power shape.

JASON Options

The JASON code presents the user several options in the input. Particularly important are options concerning weighted exposures, structure for control zones, and power flattening. JASON divides each assembly into axial layers (the number of axial layers is specified in JASON input) and determines assembly average exposure by averaging the axial layer exposures. If the user desires JASON will weight the axial layer exposures by the axial power profile when determining assembly average exposure. It was found that no axial weighting is the option for Mark 22 calculations that gives best buckling agreement.

JASON permits the user several options for control zone structure and power flattening criteria. The patch and gang control zone structures were investigated in this study. Two power flattening criteria were investigated. The two flattening options are:

1. To determine cluster powers from the average of all Mark 22 assembly powers within each cluster, and then determine control zone powers from the average of all cluster powers (denoted "JASON-2" in Figures B-1 through B-20). This is flattening option No. 2 in the INPUT.JASON.SPECS record.

2. To determine cluster powers from the maximum Mark 22 assembly power within each cluster, and then determine control zone powers from the average of all cluster powers (denoted "JASON-4" in Figures B-1 through B-40). This is flattening option No. 4 in the INPUT.JASON.SPECS record.

Observed radial power shapes (Tables B-1 and B-2) were specified to obtain the JASON results presented here for gang control zone structure (Figures B-1 through B-20).

Use of gang control zone structure without specifying radial power shape was investigated but found to give unsatisfactory results. Studying Figures B-1 through B-20 and Table B-3 it is concluded that JASON calculations with patch control zone structure and flattening option No. 4 give the most consistent results. Bias factors reported earlier were derived for this pair of options.

TABLE B-1

POWER SHAPES - FLATTENING OPTION NO. 2

CYCLE	RELATIVE POWER		
	GANG 1	GANG 2	GANG 3
C-2.1	1.000	0.966	0.881
C-2.2	1.000	0.983	0.897
C-3.1	1.000	0.997	0.831
K-6.1	1.000	1.006	0.876
K-6.2	1.000	1.001	0.874

TABLE B-2

POWER SHAPES - FLATTENING OPTION NO. 4

CYCLE	RELATIVE POWER		
	GANG 1	GANG 2	GANG 3
C-2.1	1.000	1.000	0.921
C-2.2	1.000	1.000	1.029
C-3.1	1.000	1.020	0.959
K-6.1	1.000	1.004	0.957
K-6.2	1.000	1.004	0.959

FIGURE B-3

JASON/OBSERVED BUCKLING DIFFERENCES

		ΔB^2 (OBSERVED B^2_{CR} - JASON B^2_{CR}), μB			
CYCLE	GANG	GANG-2	GANG-4	PATCH-2	PATCH-4
C-2.1	I	58	60	39	58
	II	53	67	48	65
	III	- 63	-112	48	-26
	RX	38	33	57	50
C-2.2	I	- 48	-110	- 66	-50
	II	- 21	93	- 63	-44
	III	-168	-284	24	-58
	RX	- 65	- 64	- 36	-47
C-3.1	I	70	68	68	69
	II	96	93	17	71
	III	- 47	- 32	181	64
	RX	59	59	81	70
K-6.1	I	18	22	37	27
	II	94	91	- 30	66
	III	9	7	118	43
	RX	37	37	43	42
K-6.2	I	- 41	- 41	- 48	-47
	II	- 1	- 1	-154	-50
	III	-131	-130	11	-74
	RX	- 50	- 50	- 40	-48

FIGURE B-1

C-2.1 BUCKLING IN CONTROL RODS

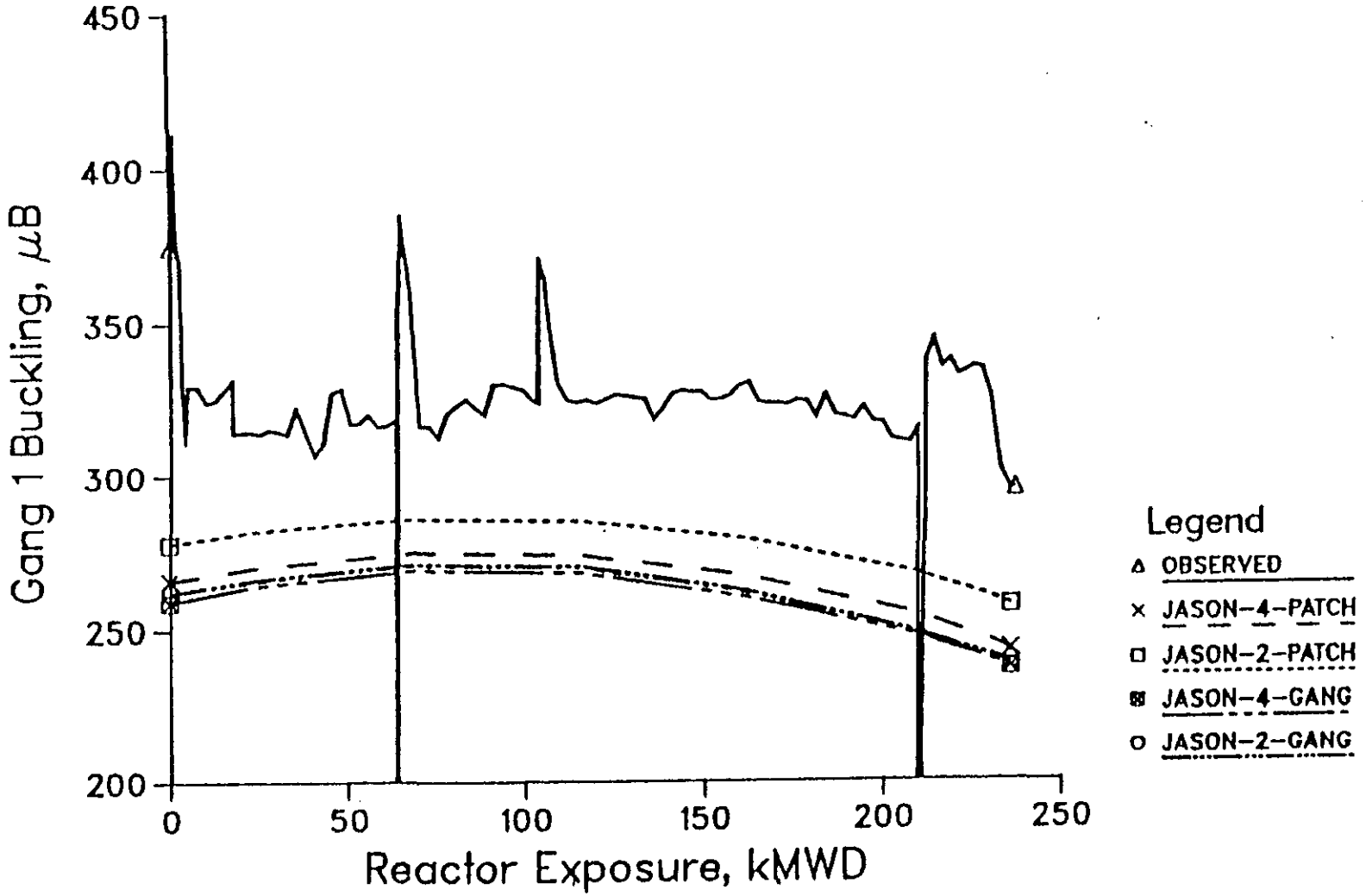

FIGURE B-2

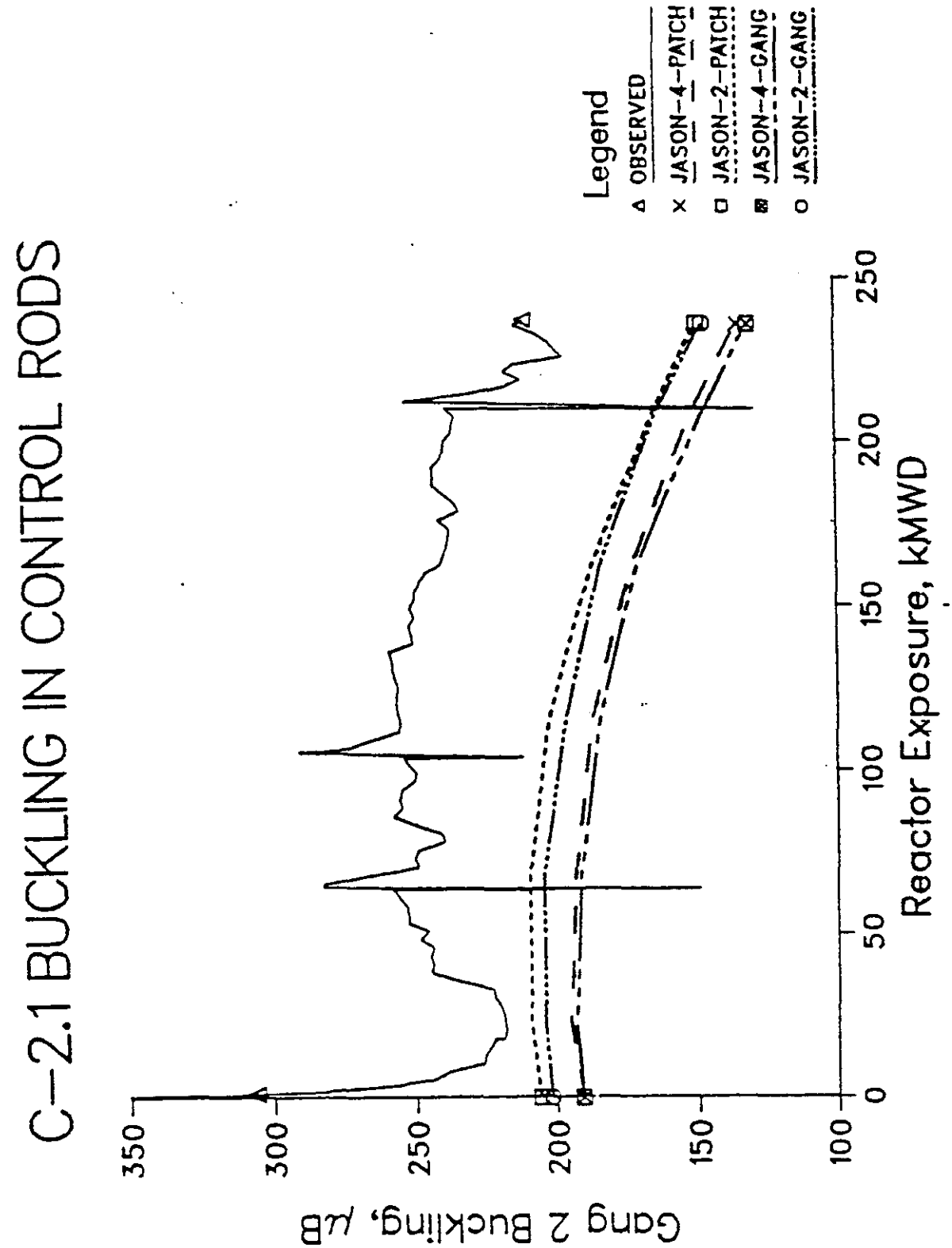
C-2.1 BUCKLING IN CONTROL RODS
Legend
OBSERVED
JASON-4-PATCH
JASON-2-PATCH
JASON-4-GANG
JASON-2-GANG
Gang 2 Buckling, μB
350
300
250
200
150
100
0
50
100
150
200
250
Reactor Exposure, kMWD

FIGURE B-3

C-2.1 BUCKLING IN CONTROL RODS

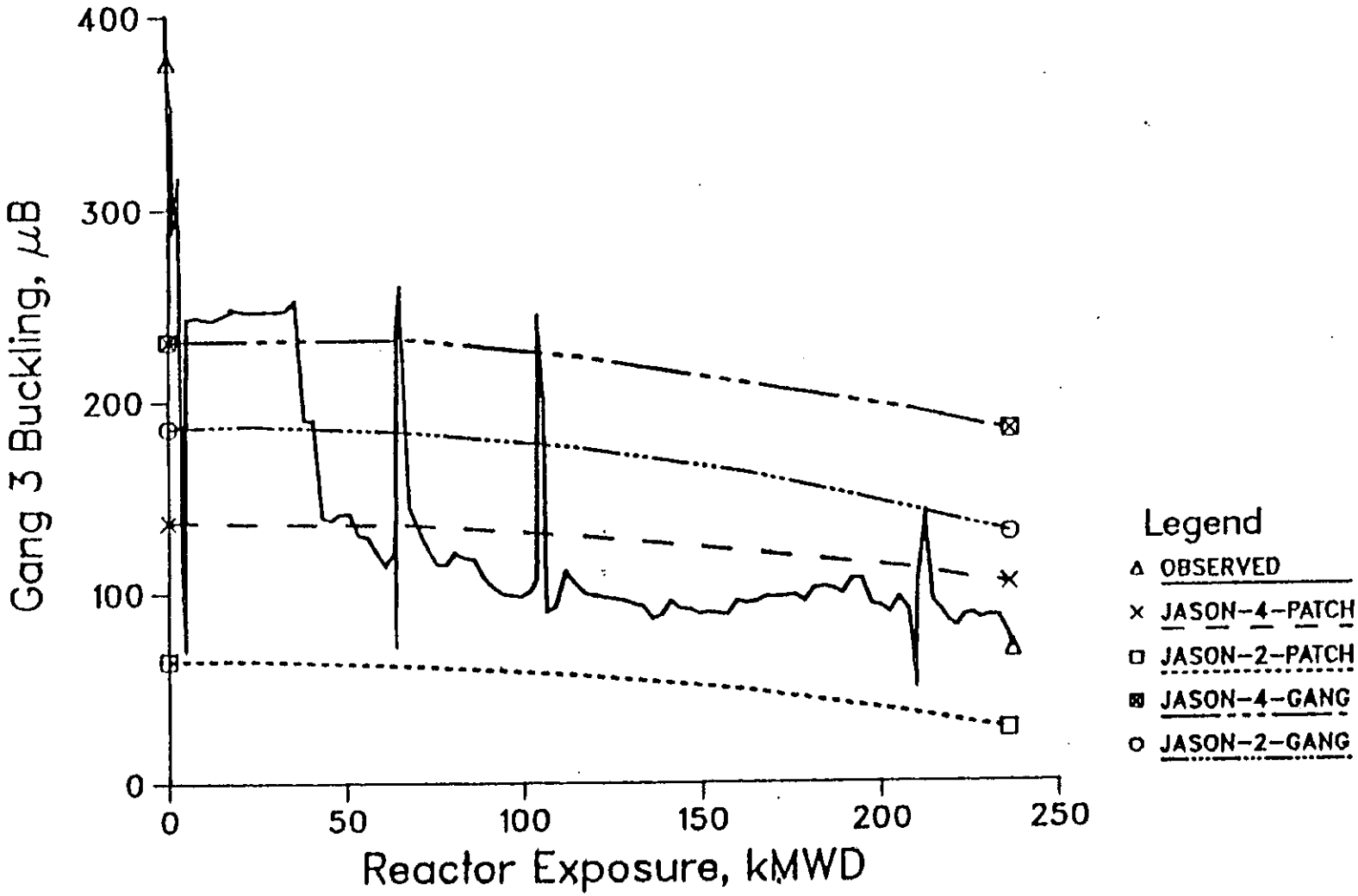

FIGURE B-4

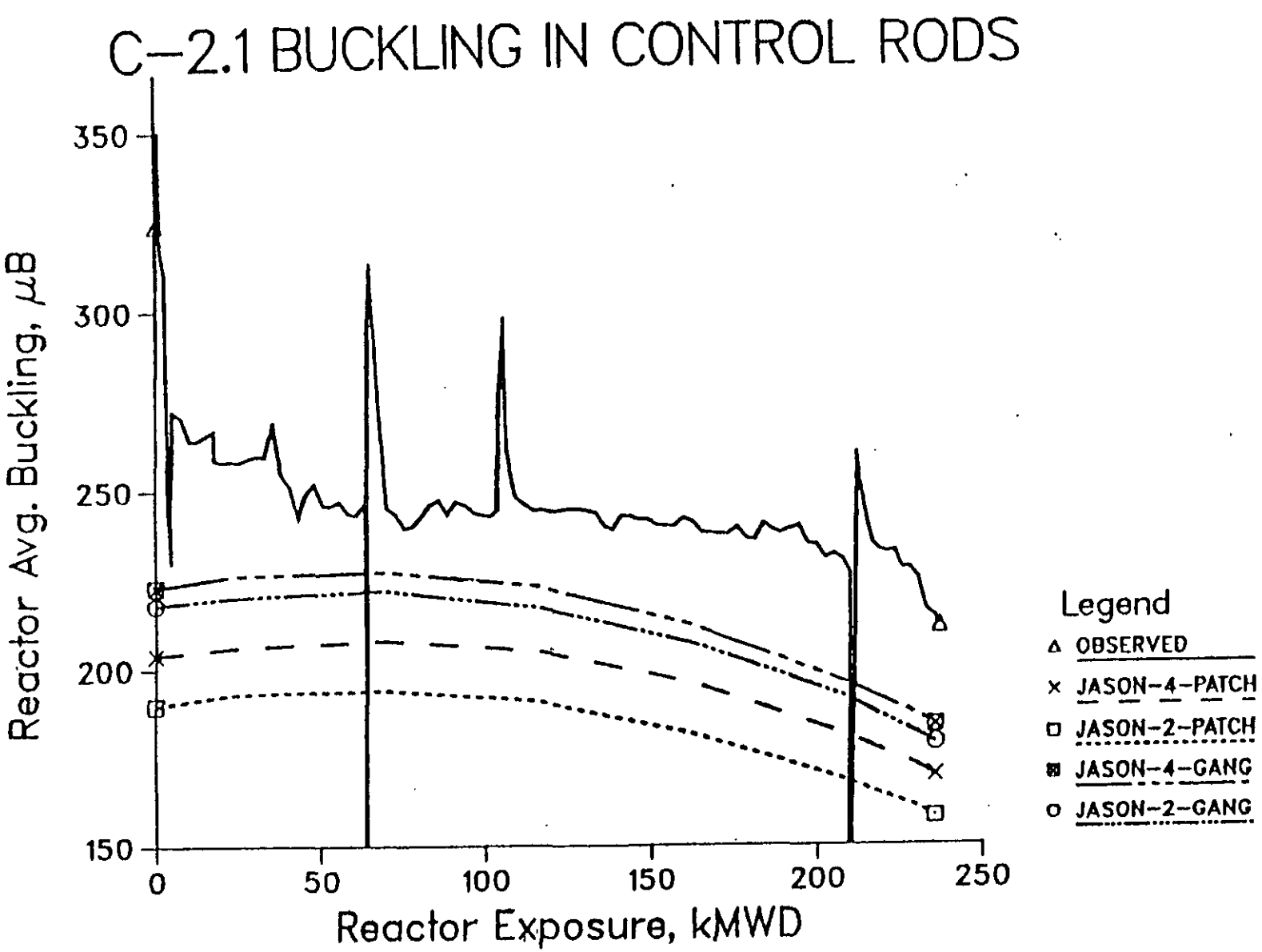
C-2.1 BUCKLING IN CONTROL RODS
Reactor Avg. Buckling, μB
350
300
250
200
150
0
50
100
150
200
250
Reactor Exposure, kMWD
Legend
OBSERVED
JASON-4-PATCH
JASON-2-PATCH
JASON-4-GANG
JASON-2-GANG

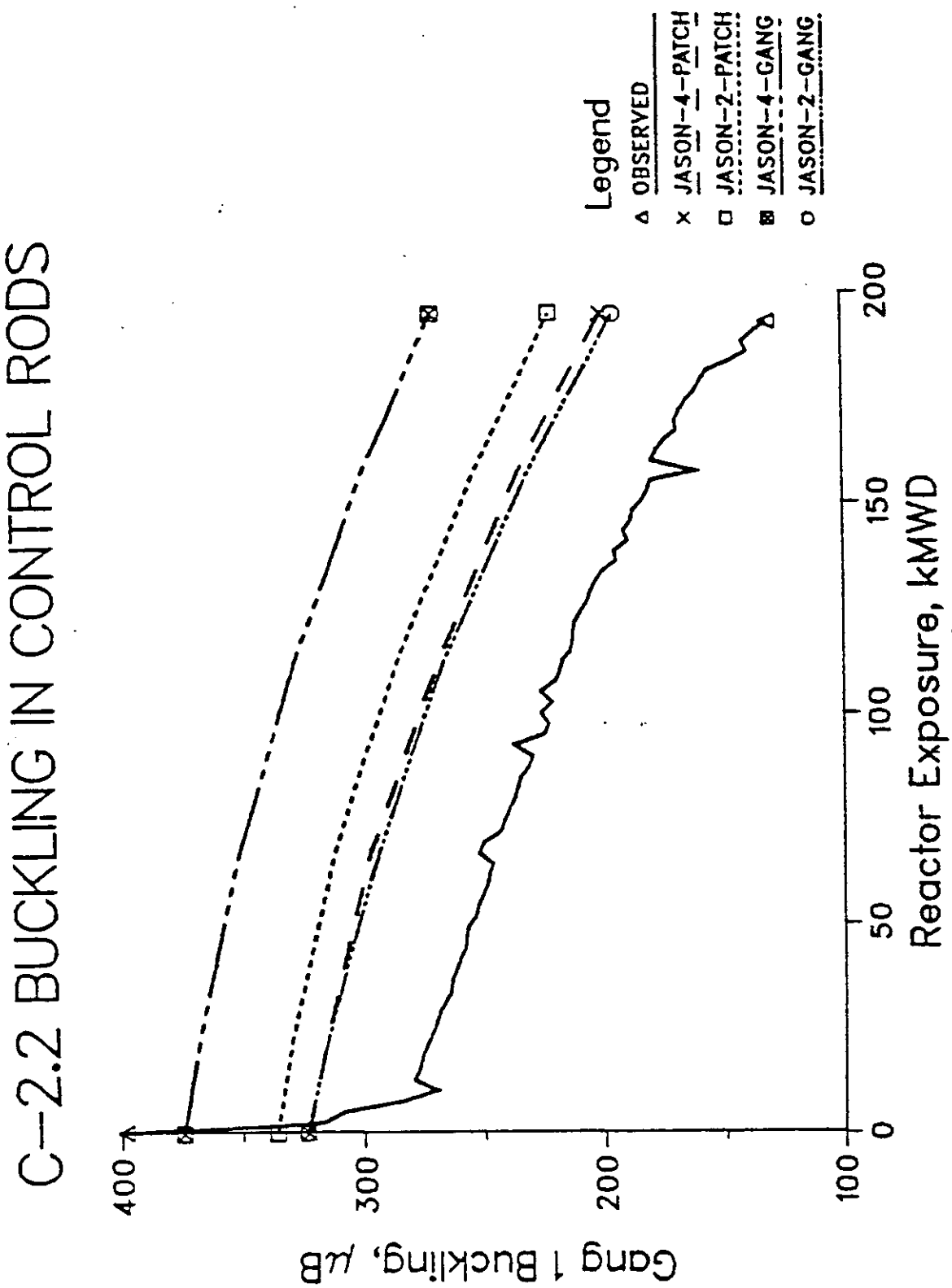
C-2.2 BUCKLING IN CONTROL RODS
Legend
OBSERVED
JASON-4-PATCH
JASON-2-PATCH
JASON-4-GANG
JASON-2-GANG
Gang 1 Buckling, μB
Reactor Exposure, kMWD
100
200
300
400
0
50
100
150
200

FIGURE B-5

FIGURE B-6

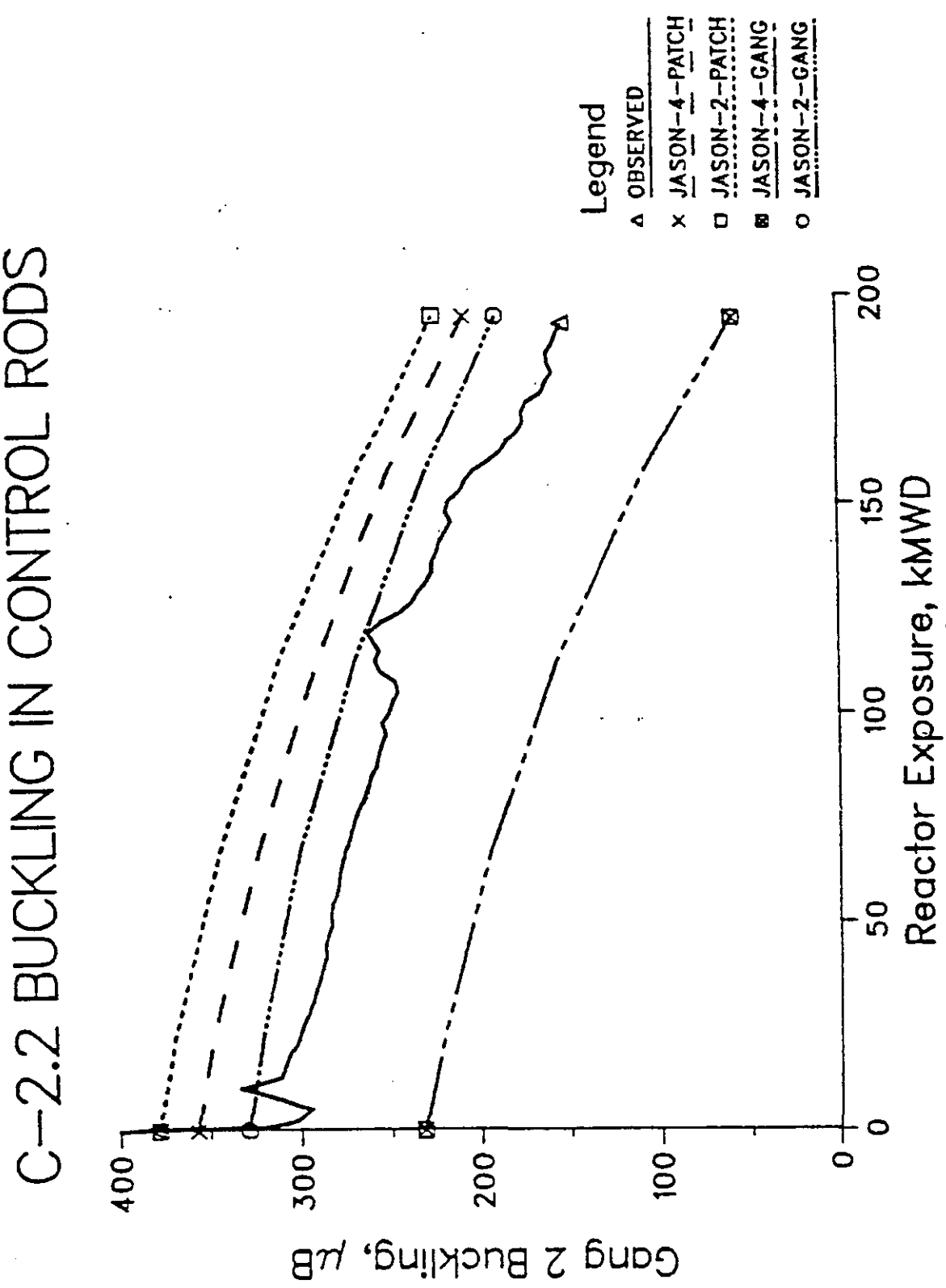
C-2.2 BUCKLING IN CONTROL RODS
Legend
OBSERVED
JASON-4-PATCH
JASON-2-PATCH
JASON-4-GANG
JASON-2-GANG
Gang 2 Buckling, μB
400
300
200
100
0
0
50
100
150
200
Reactor Exposure, kMWD

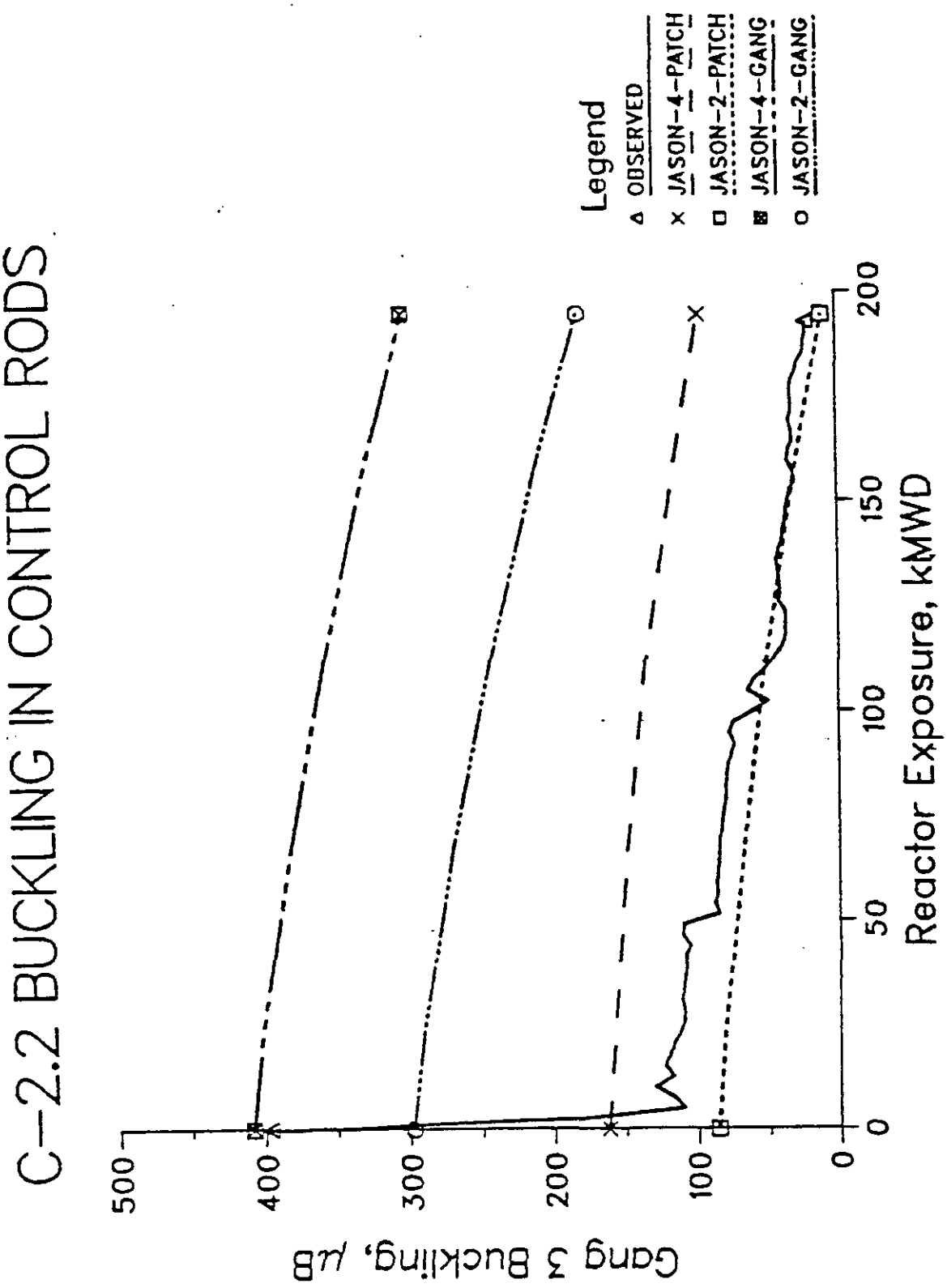
C-2.2 BUCKLING IN CONTROL RODS
Legend
OBSERVED
JASON-4-PATCH
JASON-2-PATCH
JASON-4-GANG
JASON-2-GANG
Gang 3 Buckling, μB
500
400
300
200
100
0
0
50
100
150
200
Reactor Exposure, kMWD

FIGURE B-7

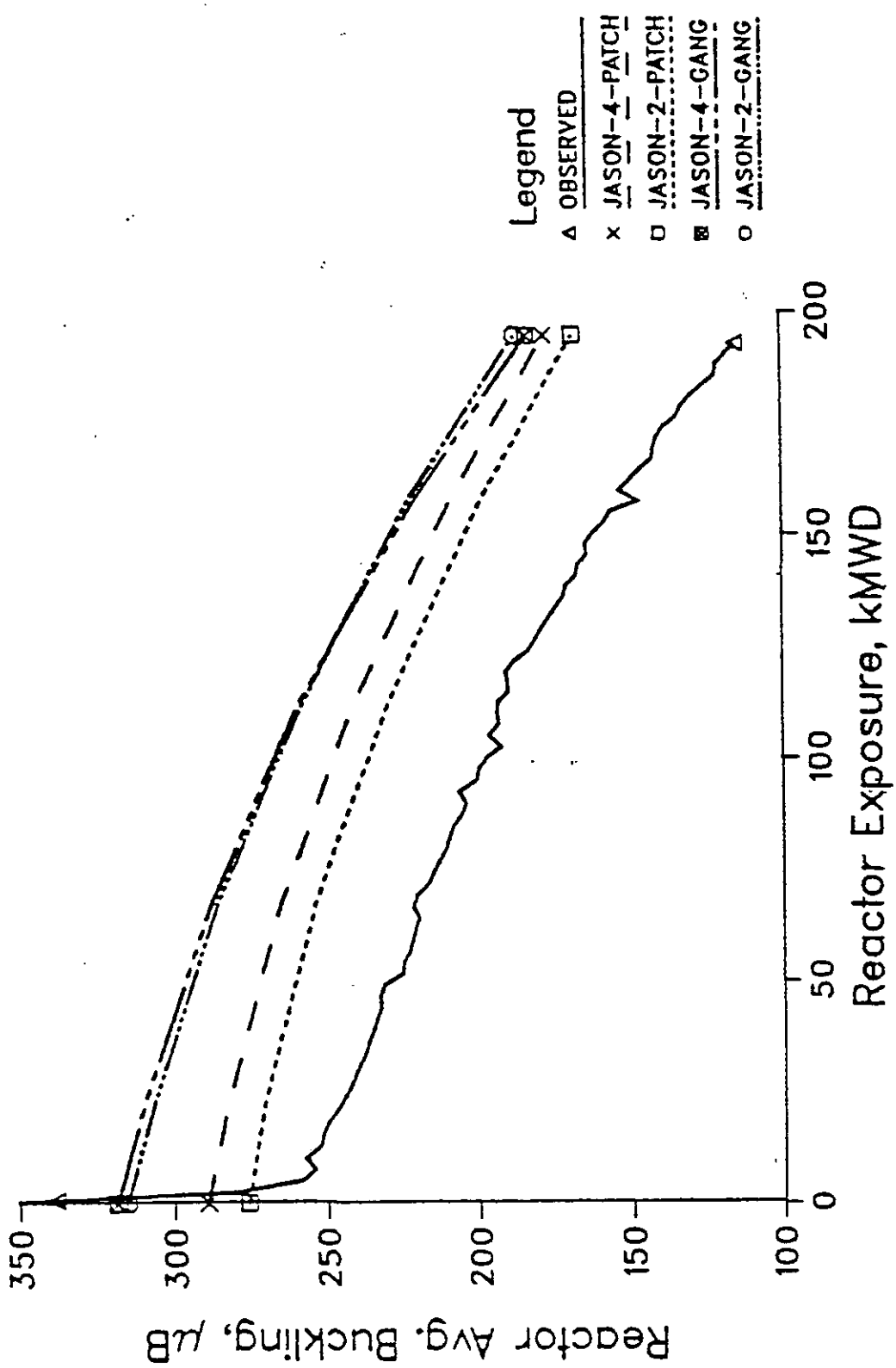
C-2.2 BUCKLING IN CONTROL RODS
Legend
OBSERVED
JASON-4-PATCH
JASON-2-PATCH
JASON-4-GANG
JASON-2-GANG
Reactor Avg. Buckling, μB
Reactor Exposure, kMWD
350
300
250
200
150
100
0
50
100
150
200

FIGURE 8-8

FIGURE B-9

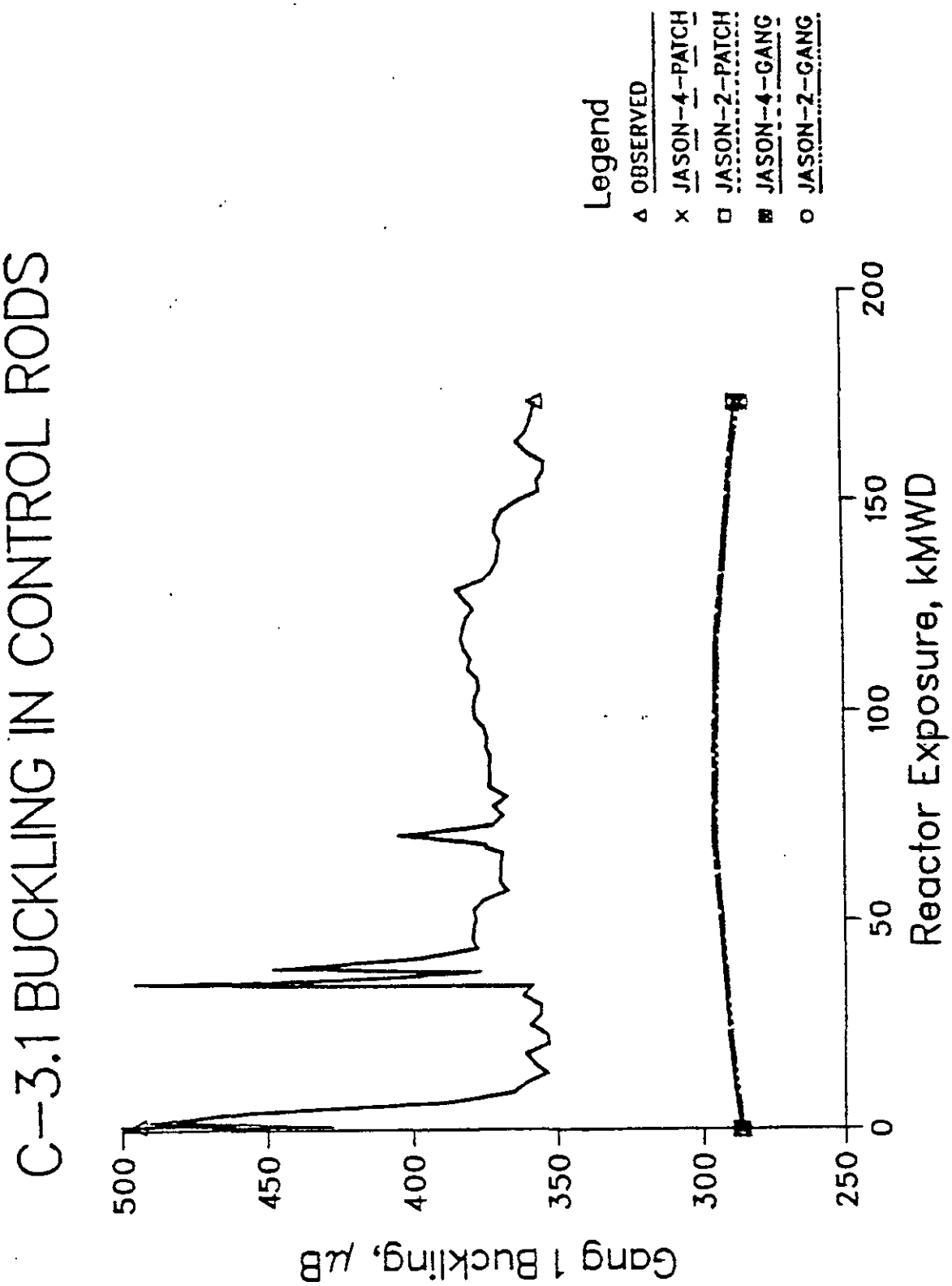
C-3.1 BUCKLING IN CONTROL RODS
Legend
OBSERVED
JASON-4-PATCH
JASON-2-PATCH
JASON-4-GANG
JASON-2-GANG
Gang 1 Buckling, μB^2
500
450
400
350
300
250
0
50
100
150
200
Reactor Exposure, kMWD

FIGURE B-10

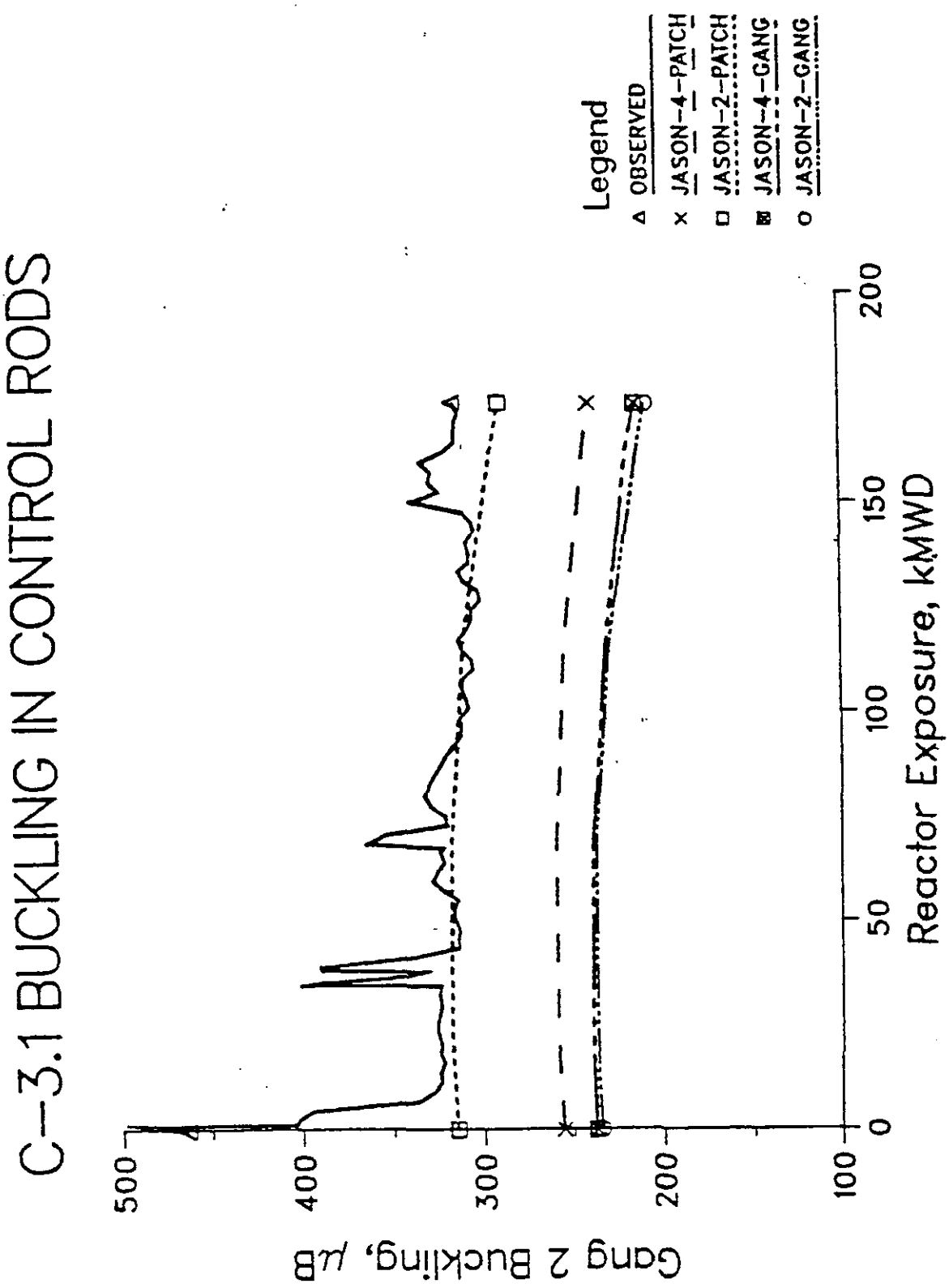
C-3.1 BUCKLING IN CONTROL RODS
Legend
OBSERVED
JASON-4-PATCH
JASON-2-PATCH
JASON-4-GANG
JASON-2-GANG
Gang 2 Buckling, μB
500
400
300
200
100
0
50
100
150
200
Reactor Exposure, kMWD

FIGURE B-11

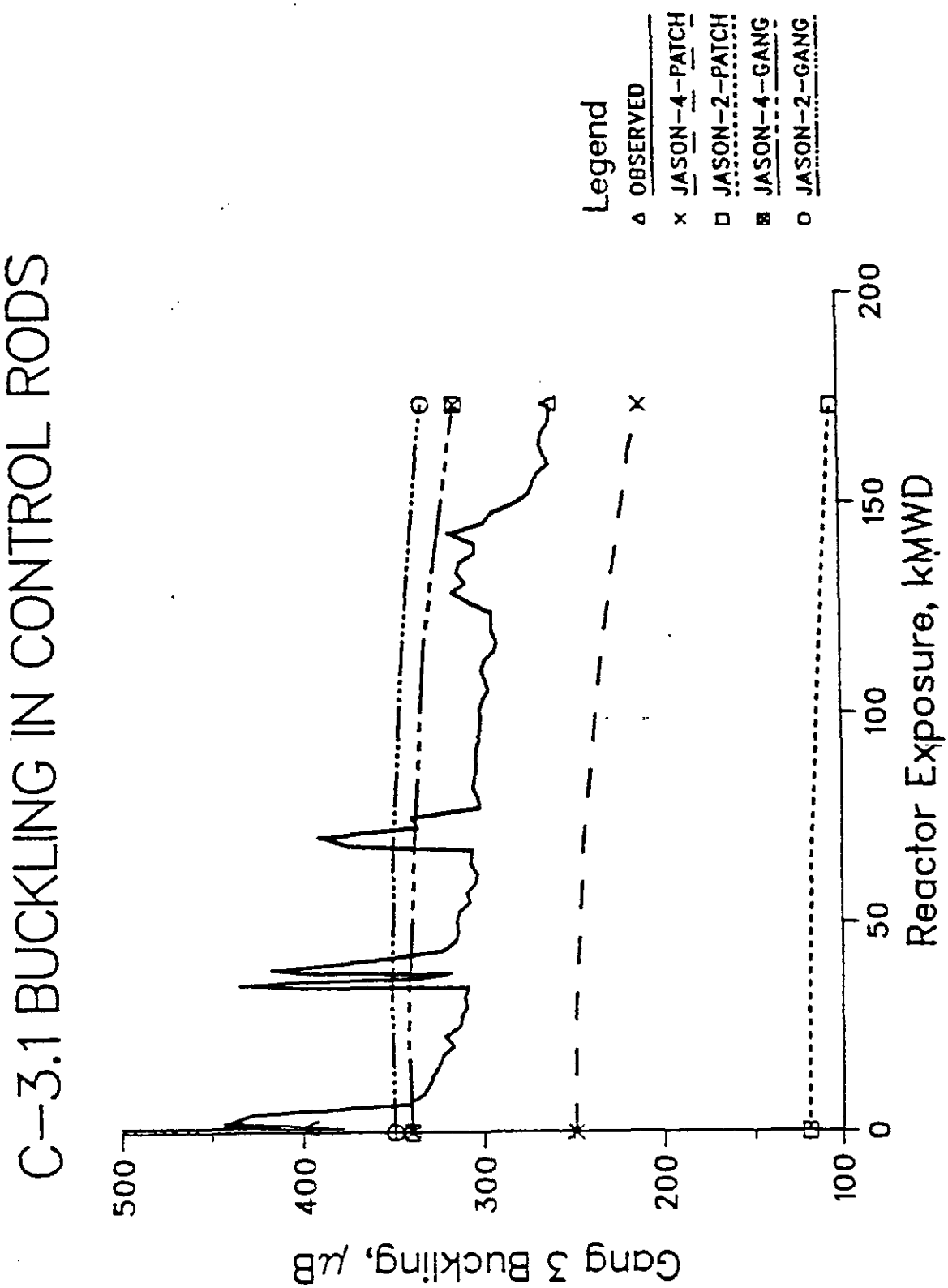
C-3.1 BUCKLING IN CONTROL RODS
Legend
OBSERVED
JASON-4-PATCH
JASON-2-PATCH
JASON-4-GANG
JASON-2-GANG
Gang 3 Buckling, μB
500
400
300
200
100
0
50
100
150
200
Reactor Exposure, kMWD

FIGURE B-12

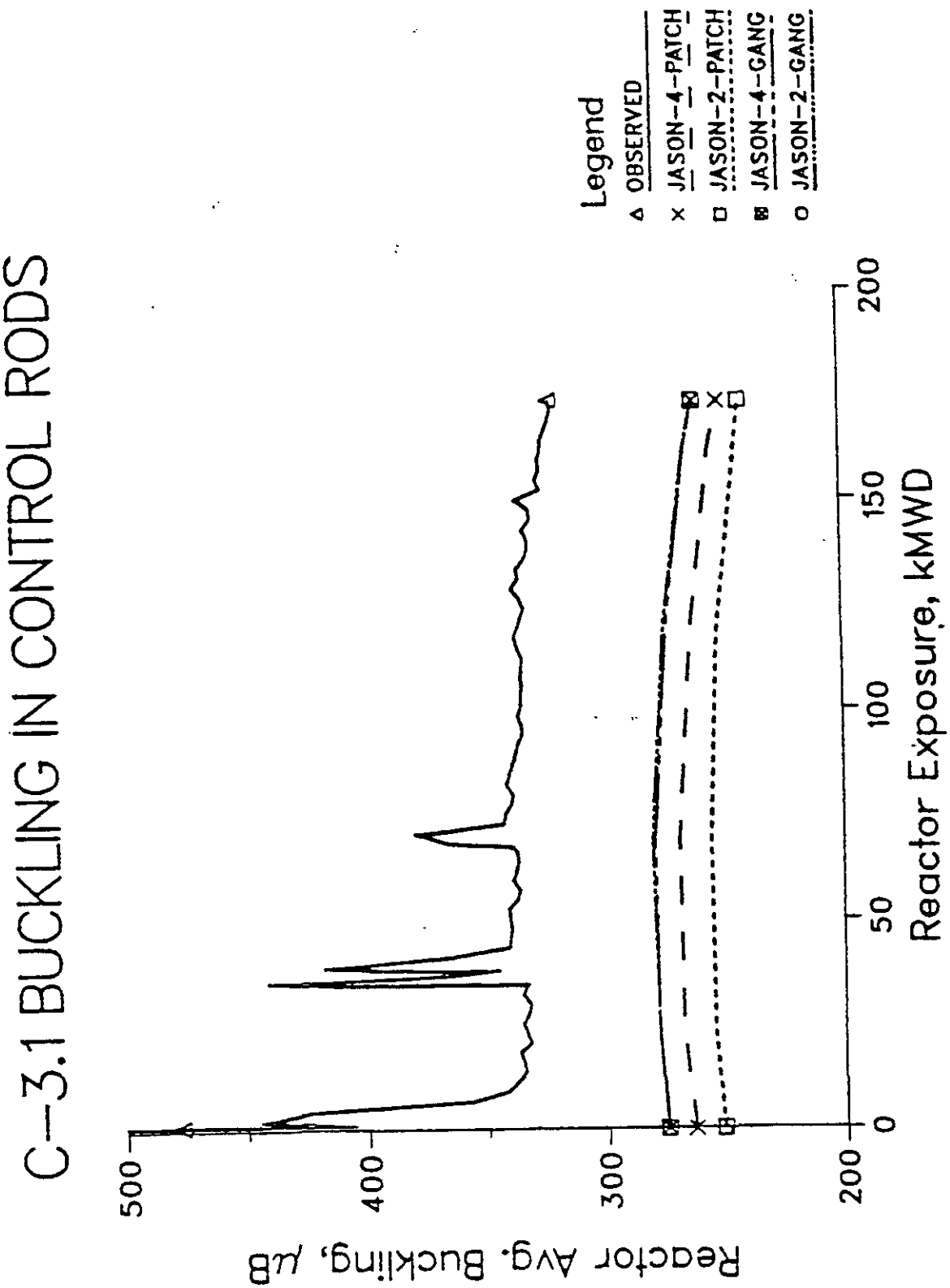
C-3.1 BUCKLING IN CONTROL RODS
Legend
OBSERVED
JASON-4-PATCH
JASON-2-PATCH
JASON-4-GANG
JASON-2-GANG
Reactor Avg. Buckling, μB
500
400
300
200
0
50
100
150
200
Reactor Exposure, kMWD

FIGURE B-13

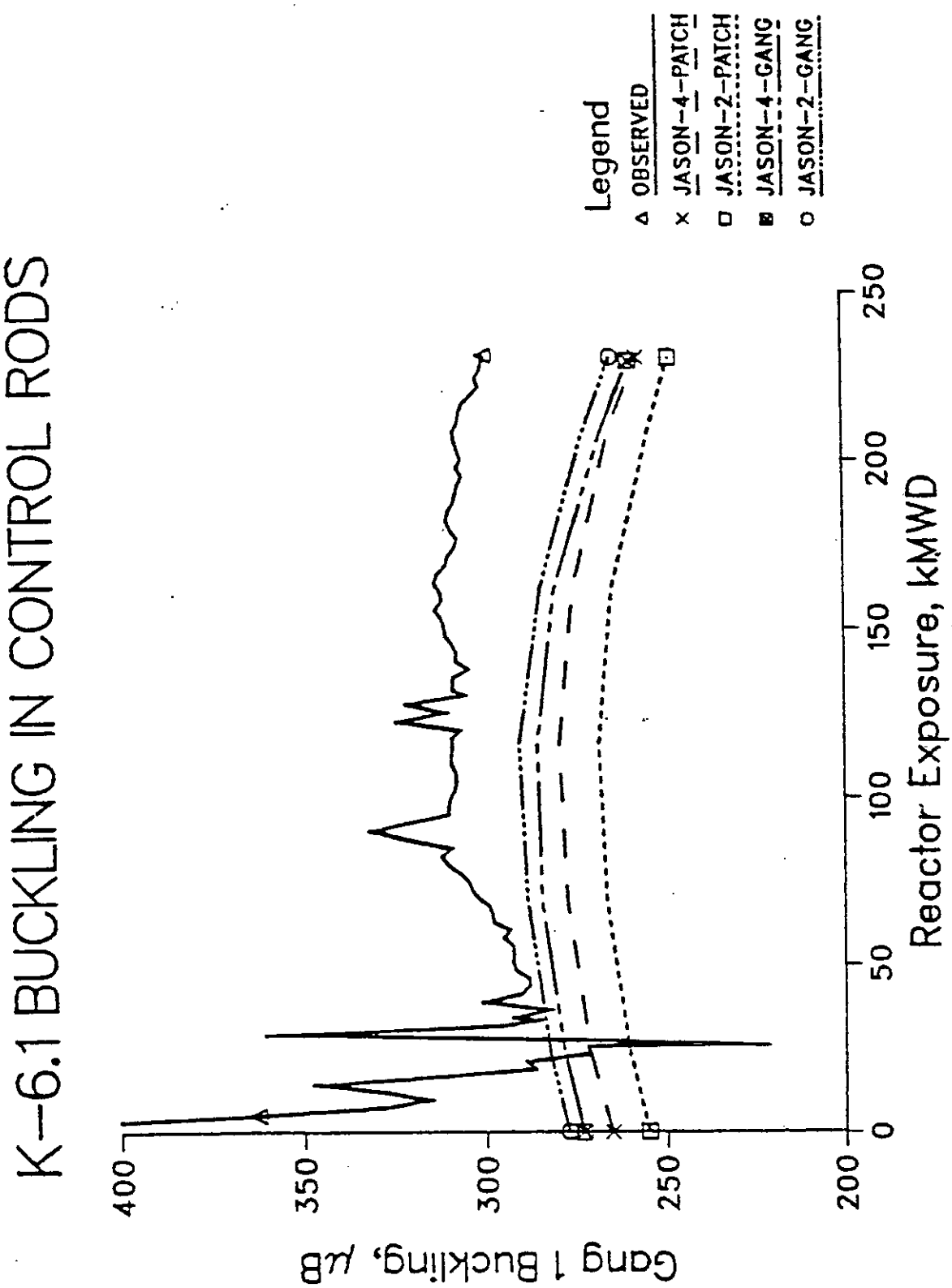
K-6.1 BUCKLING IN CONTROL RODS
Legend
OBSERVED
JASON-4-PATCH
JASON-2-PATCH
JASON-4-GANG
JASON-2-GANG
Gang 1 Buckling, $\mathcal{M}B$
Reactor Exposure, kMWD
400
350
300
250
200
0
50
100
150
200
250

FIGURE B-14

K-6.1 BUCKLING IN CONTROL RODS

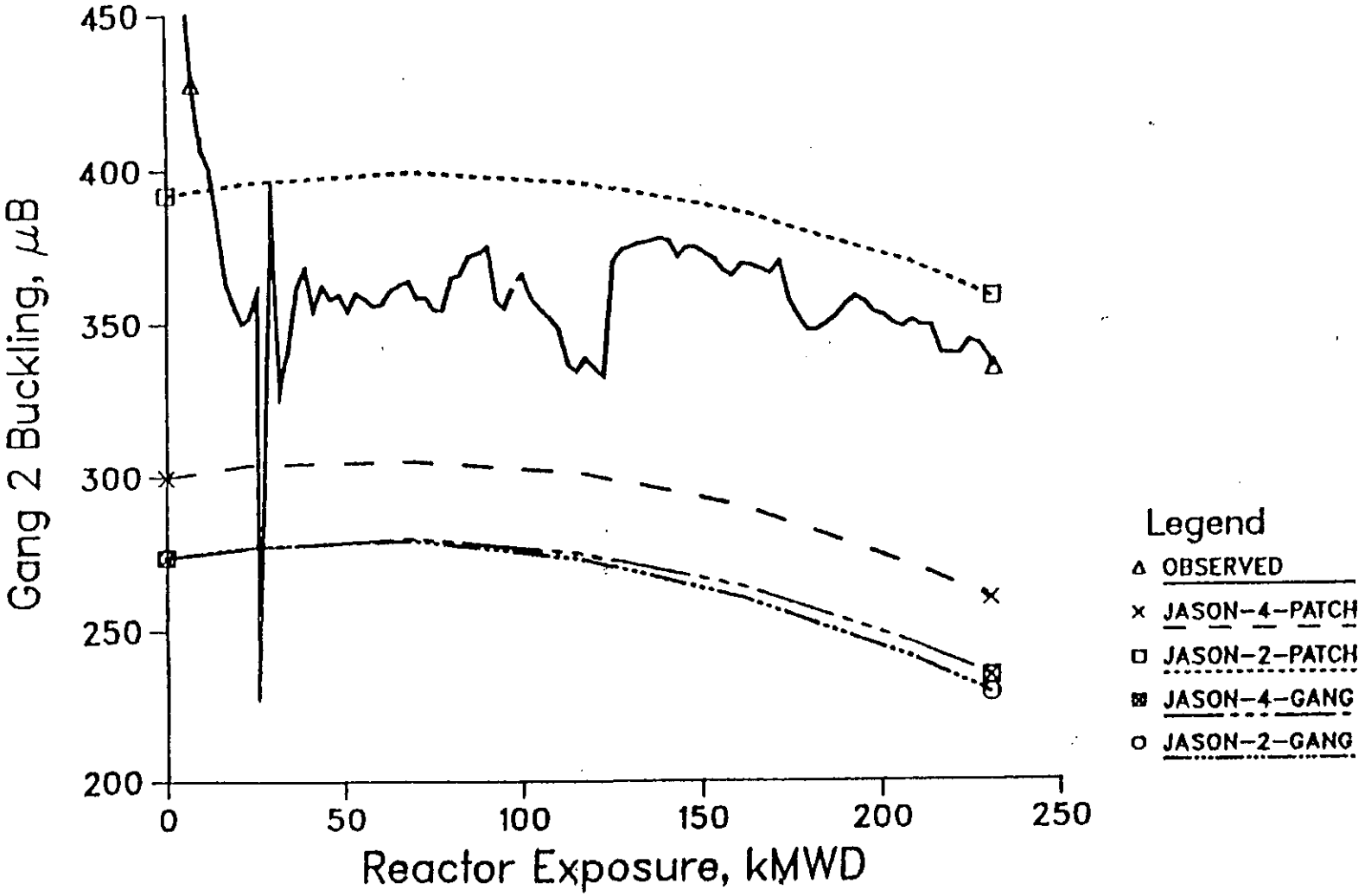

FIGURE B-15

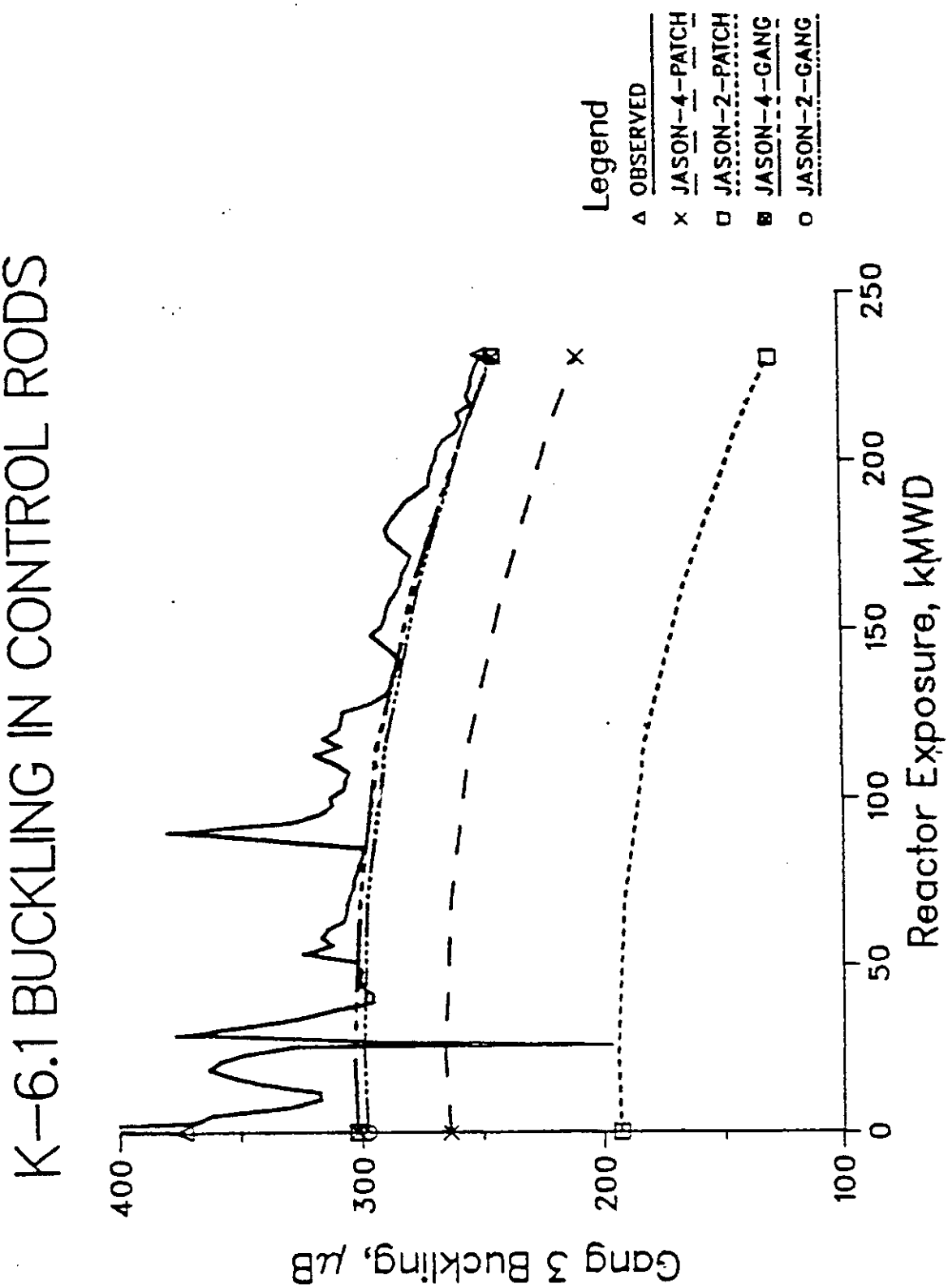
K-6.1 BUCKLING IN CONTROL RODS
Legend
OBSERVED
JASON-4-PATCH
JASON-2-PATCH
JASON-4-GANG
JASON-2-GANG
Gang 3 Buckling, μB
Reactor Exposure, kMWD
400
300
200
100
0
50
100
150
200
250

FIGURE B-16

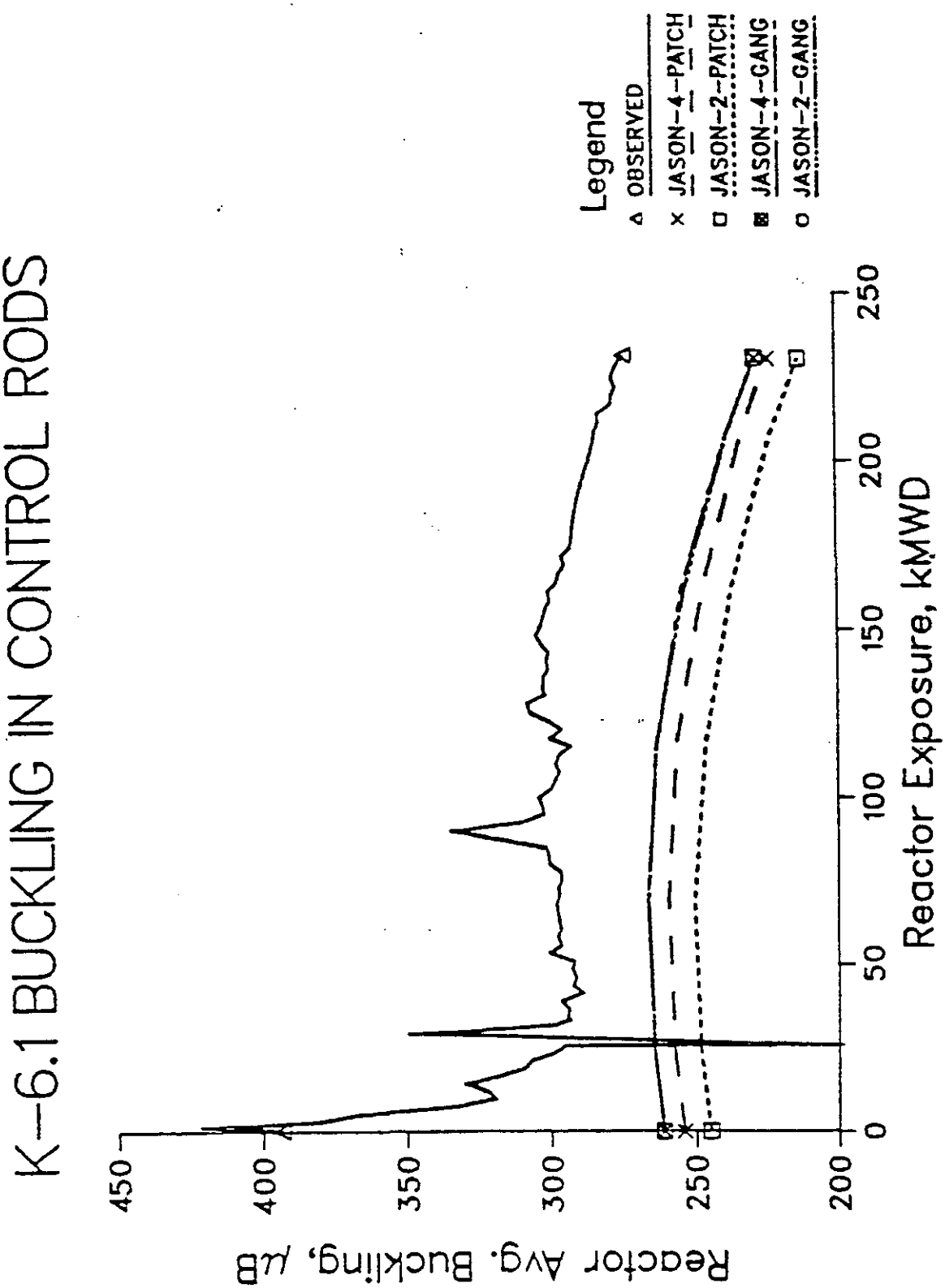
K-6.1 BUCKLING IN CONTROL RODS
Legend
OBSERVED
JASON-4-PATCH
JASON-2-PATCH
JASON-4-GANG
JASON-2-GANG
Reactor Avg. Buckling, μB
Reactor Exposure, kMWD
450
400
350
300
250
200
0
50
100
150
200
250

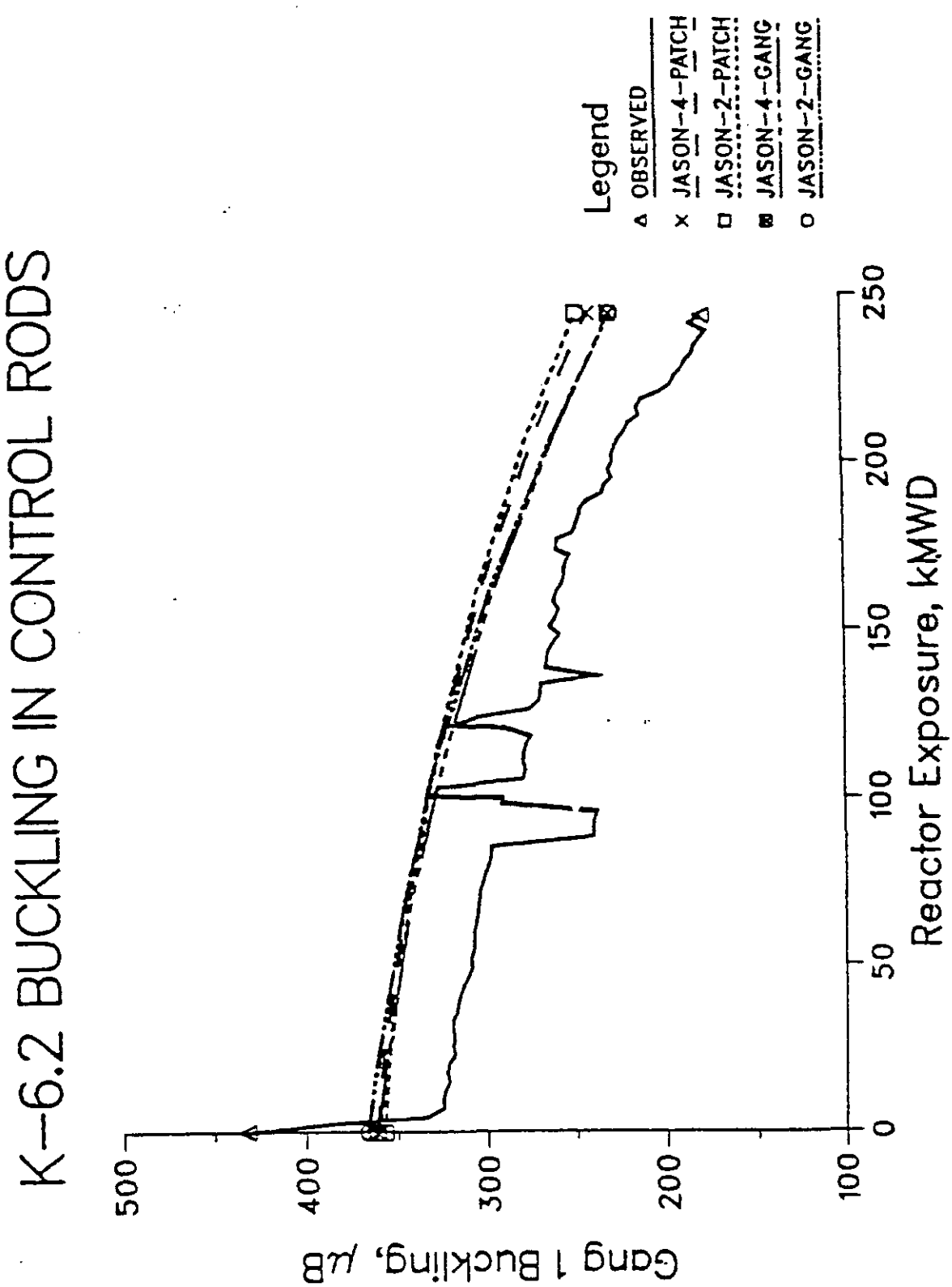
K-6.2 BUCKLING IN CONTROL RODS
Legend
OBSERVED
JASON-4-PATCH
JASON-2-PATCH
JASON-4-GANG
JASON-2-GANG
Gang 1 Buckling, μB
Reactor Exposure, kMWD
100
200
300
400
500
0
50
100
150
200
250

FIGURE B-17

FIGURE B-18

K-6.2 BUCKLING IN CONTROL RODS

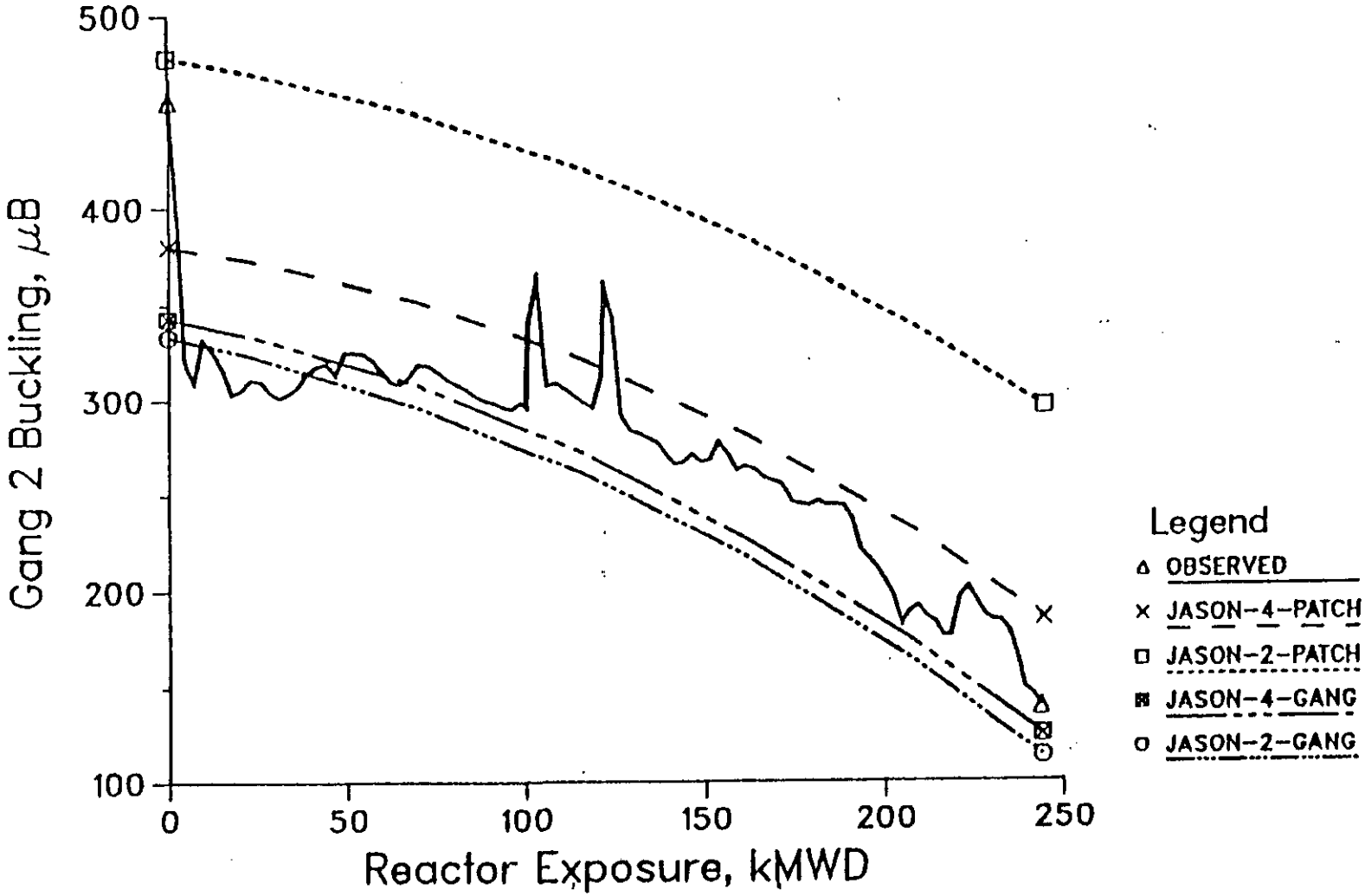

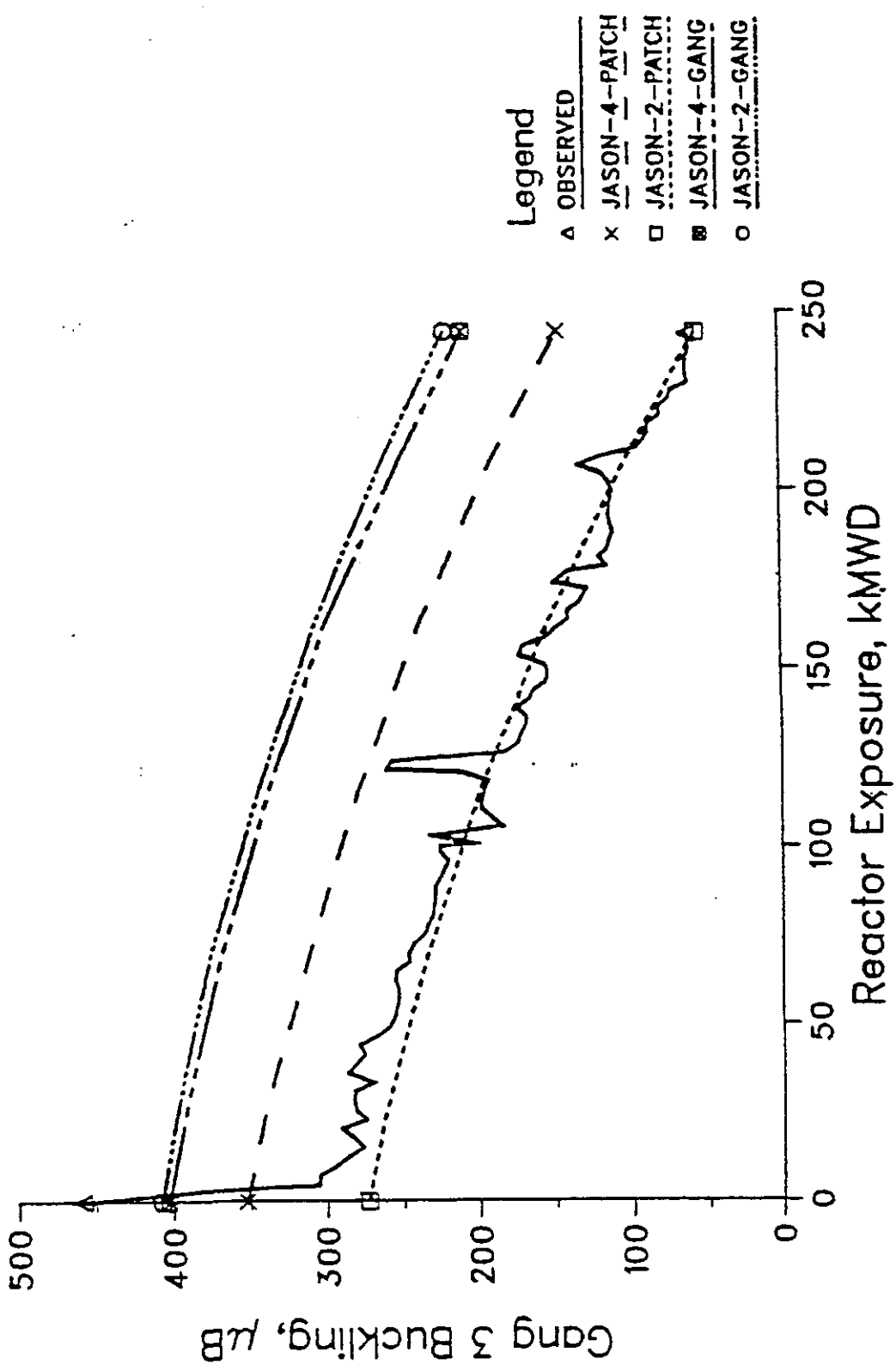
K-6.2 BUCKLING IN CONTROL RODS
Legend
OBSERVED
JASON-4-PATCH
JASON-2-PATCH
JASON-4-GANG
JASON-2-GANG
Gang 3 Buckling, μB
500
400
300
200
100
0
0
50
100
150
200
250
Reactor Exposure, kMWD

FIGURE 8-19

FIGURE B-20

K-6.2 BUCKLING IN CONTROL RODS

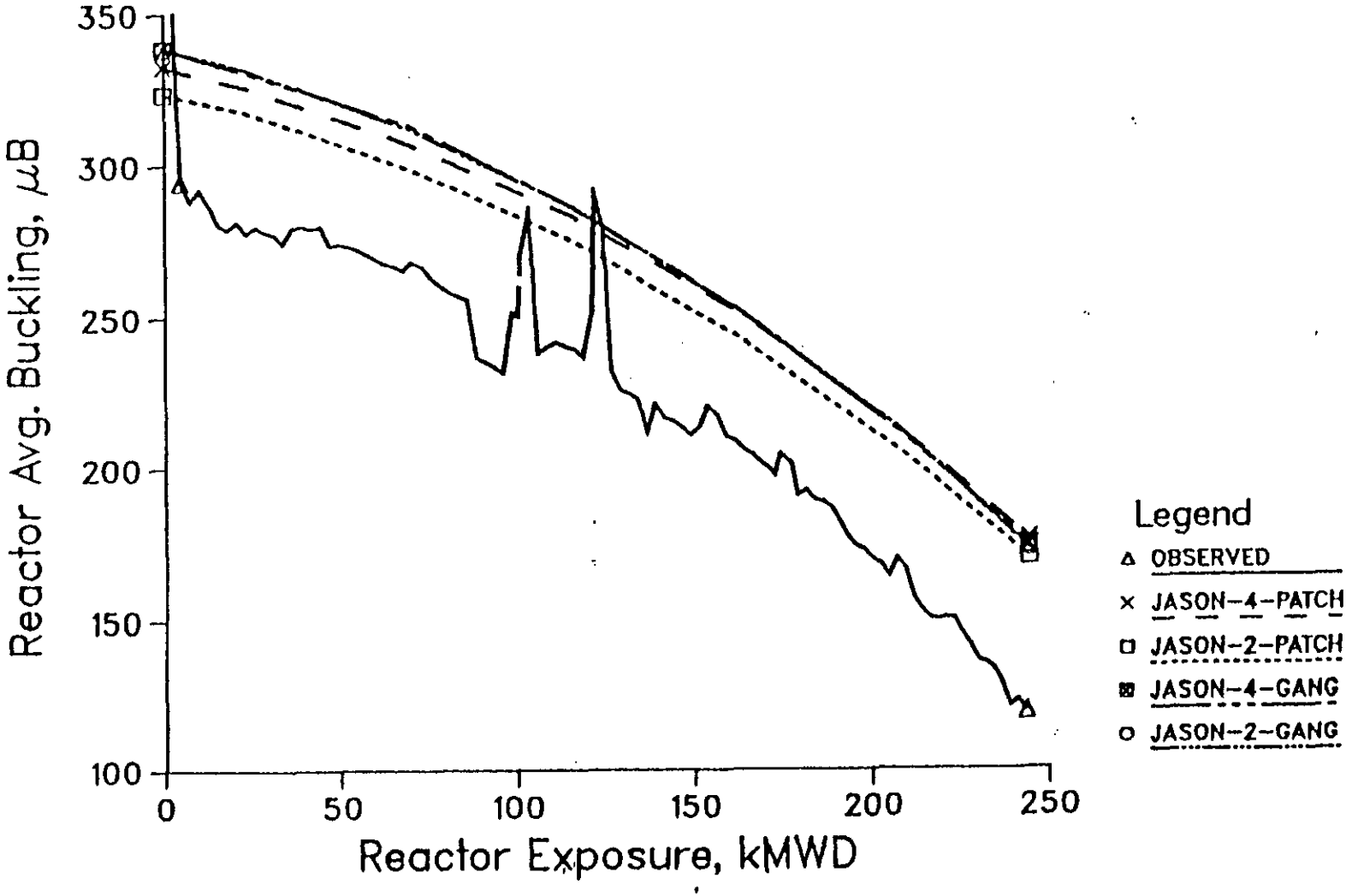

FIGURE B-21

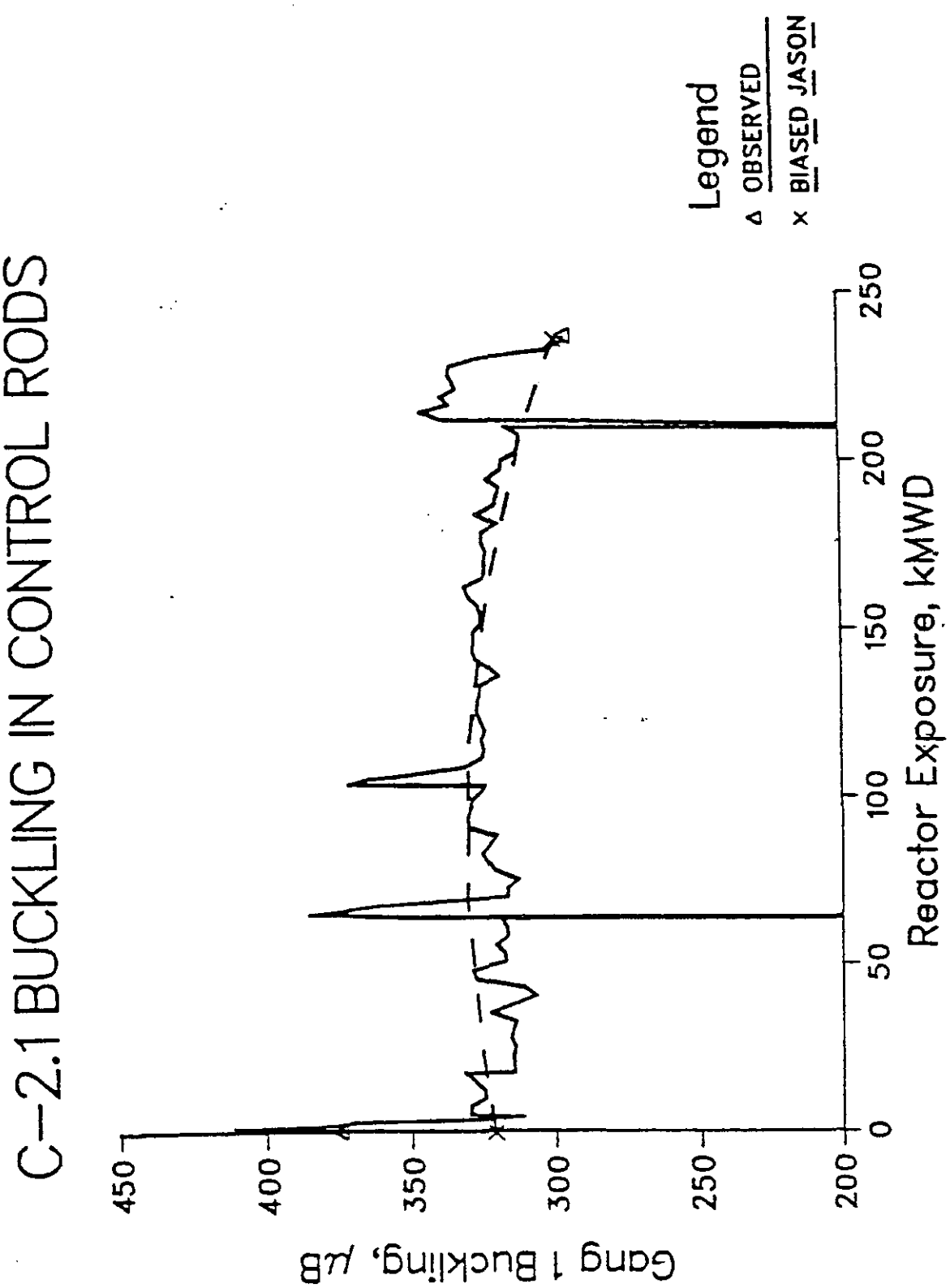
C-2.1 BUCKLING IN CONTROL RODS
Legend
△ OBSERVED
× BIASED JASON
Gang 1 Buckling, πB
450
400
350
300
250
200
0
50
100
150
200
250
Reactor Exposure, kMWD

FIGURE B-22

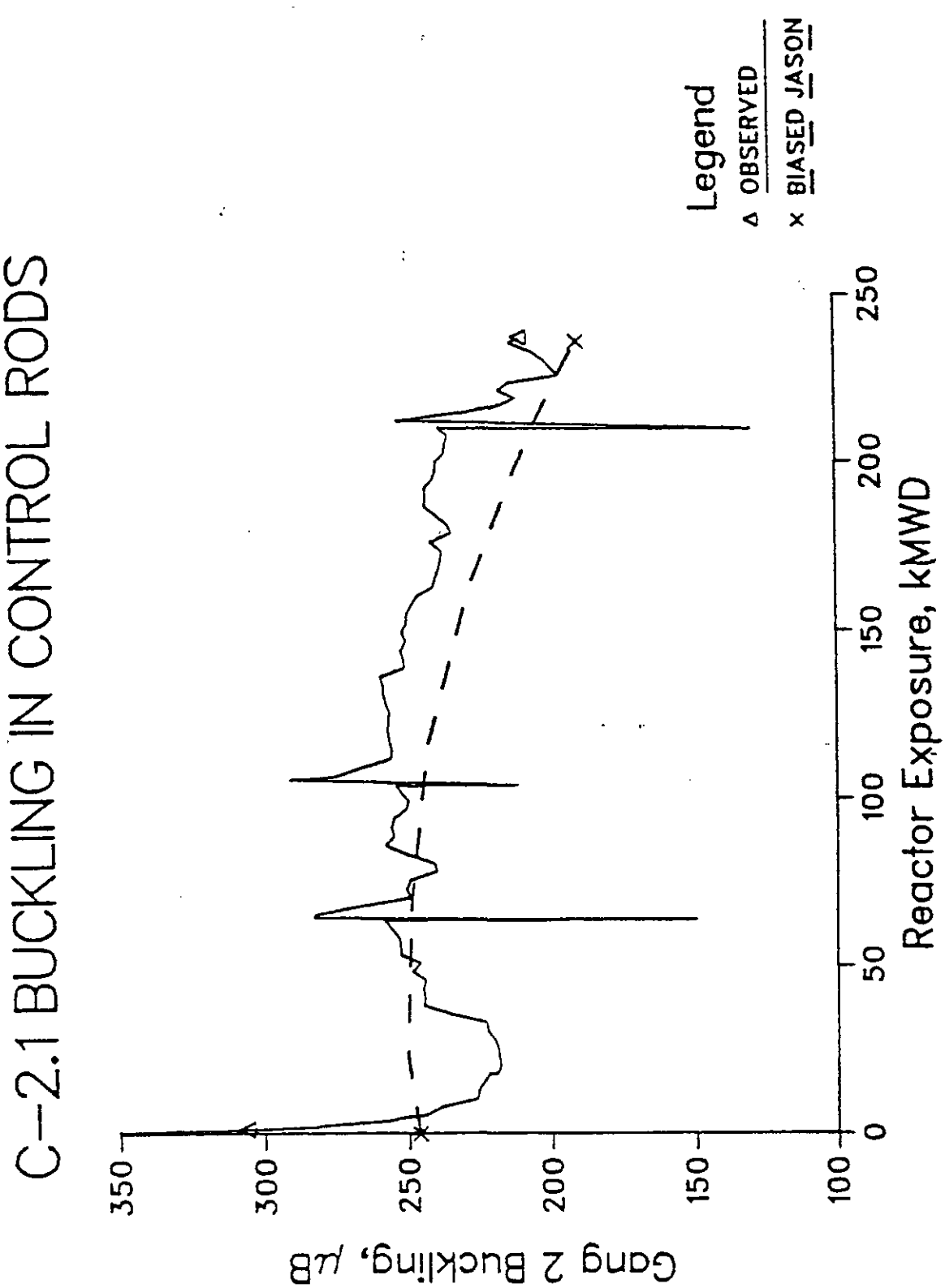
C-2.1 BUCKLING IN CONTROL RODS
Legend
△ OBSERVED
× BIASED JASON
Gang 2 Buckling, μB
350
300
250
200
150
100
0
50
100
150
200
250
Reactor Exposure, kMWD

FIGURE B-23

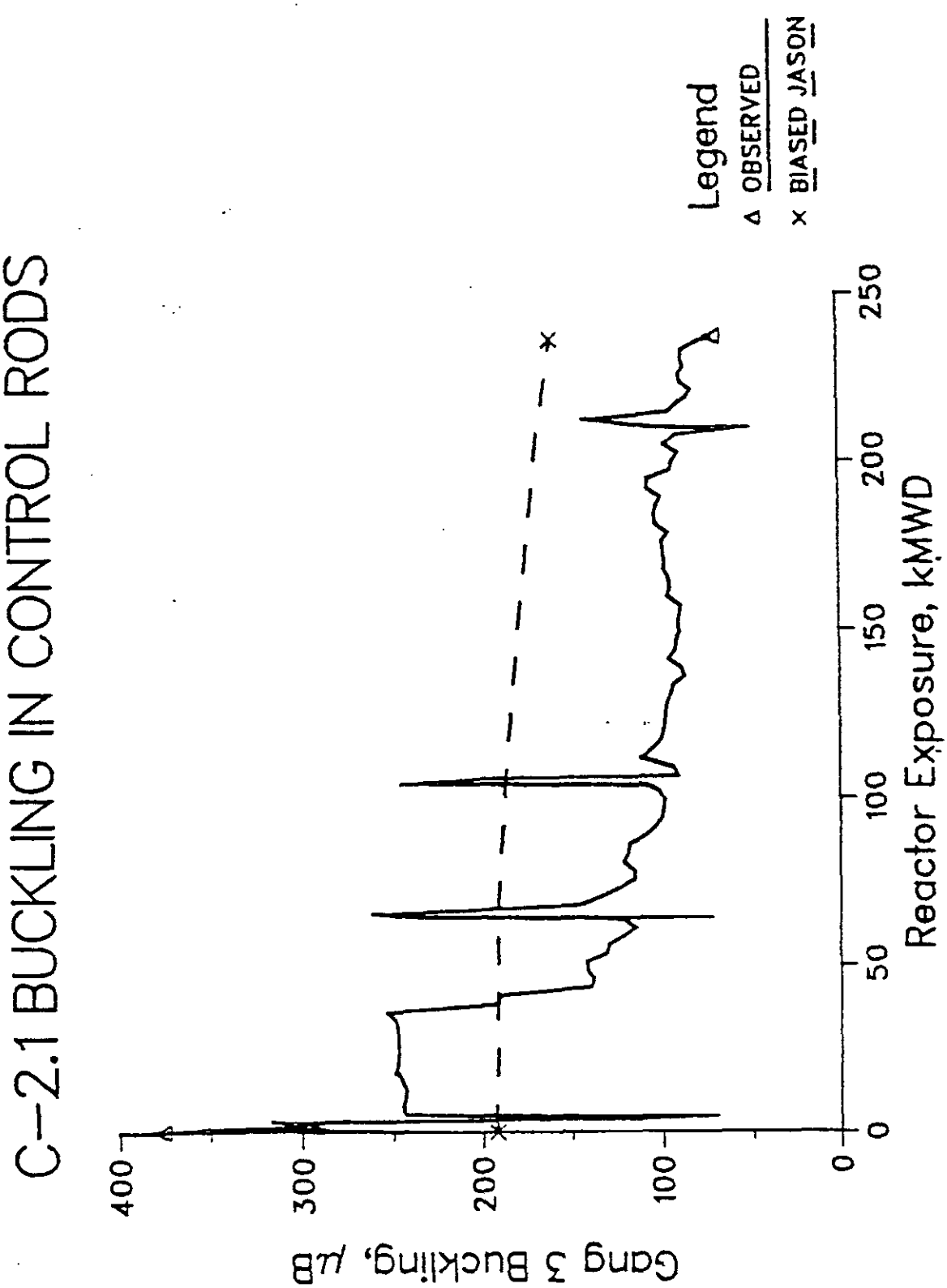
C-2.1 BUCKLING IN CONTROL RODS
Legend
△ OBSERVED
× BIASED JASON
Gang 3 Buckling, μB
400
300
200
100
0
0
50
100
150
200
250
Reactor Exposure, kMWD

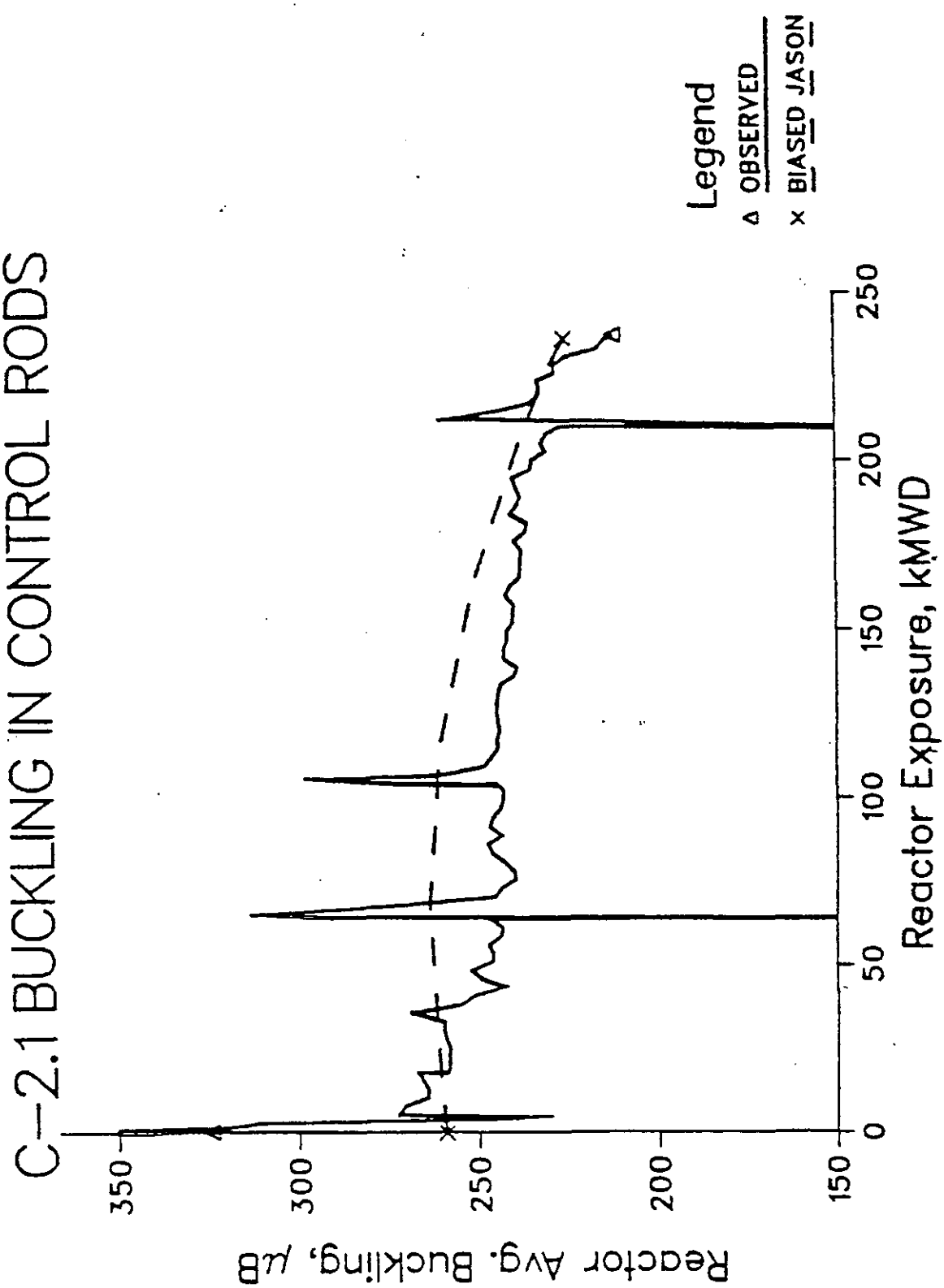
C-2.1 BUCKLING IN CONTROL RODS
Legend
△ OBSERVED
× BIASED JASON
Reactor Avg. Buckling, μB
350
300
250
200
150
0
50
100
150
200
250
Reactor Exposure, kMWD

FIGURE B-24

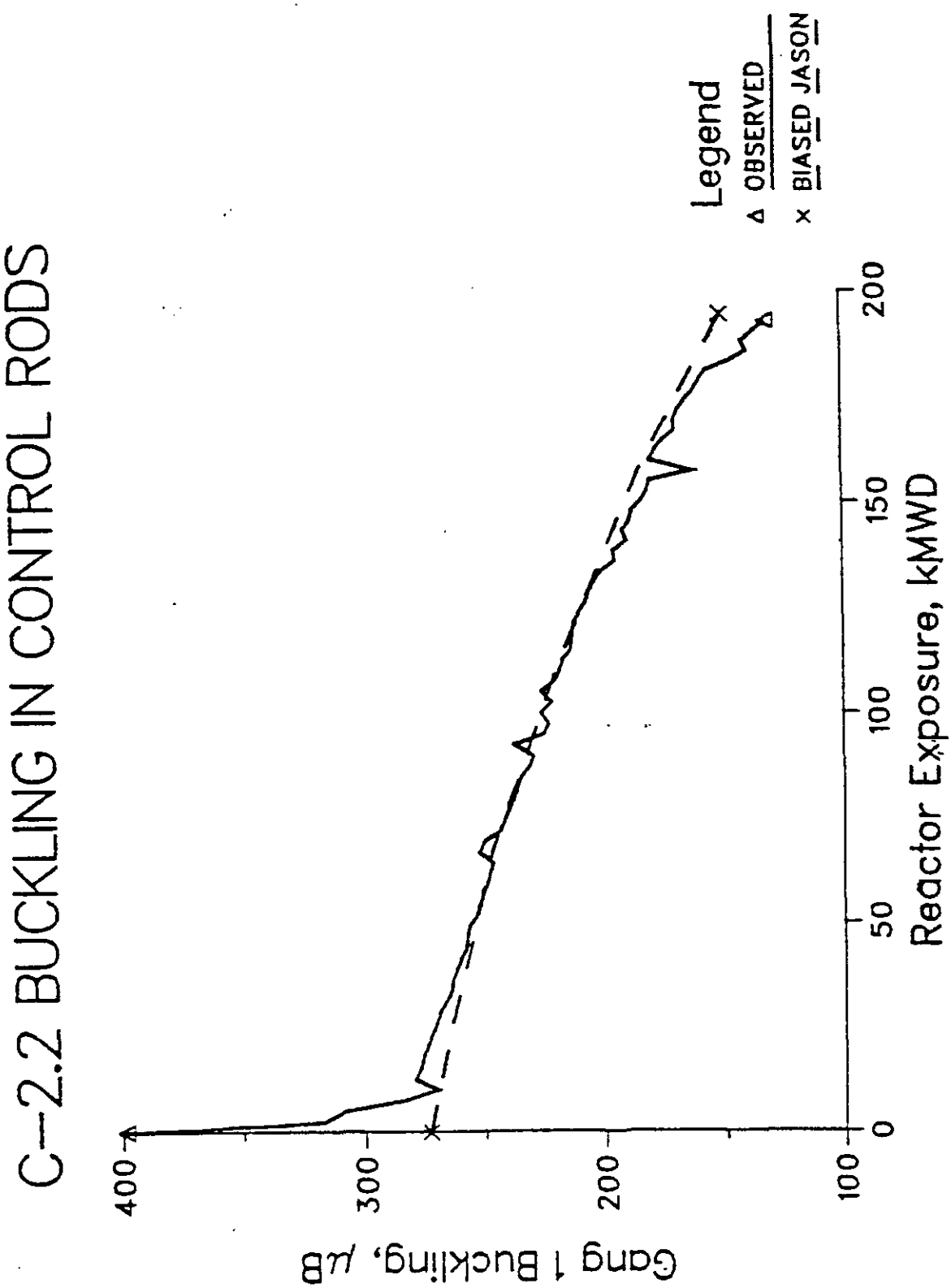
C-2.2 BUCKLING IN CONTROL RODS
Legend
Δ OBSERVED
× BIASED JASON
Gang 1 Buckling, μB
400
300
200
100
0
50
100
150
200
Reactor Exposure, kMWD

FIGURE B-25

FIGURE B-26

C-2.2 BUCKLING IN CONTROL RODS

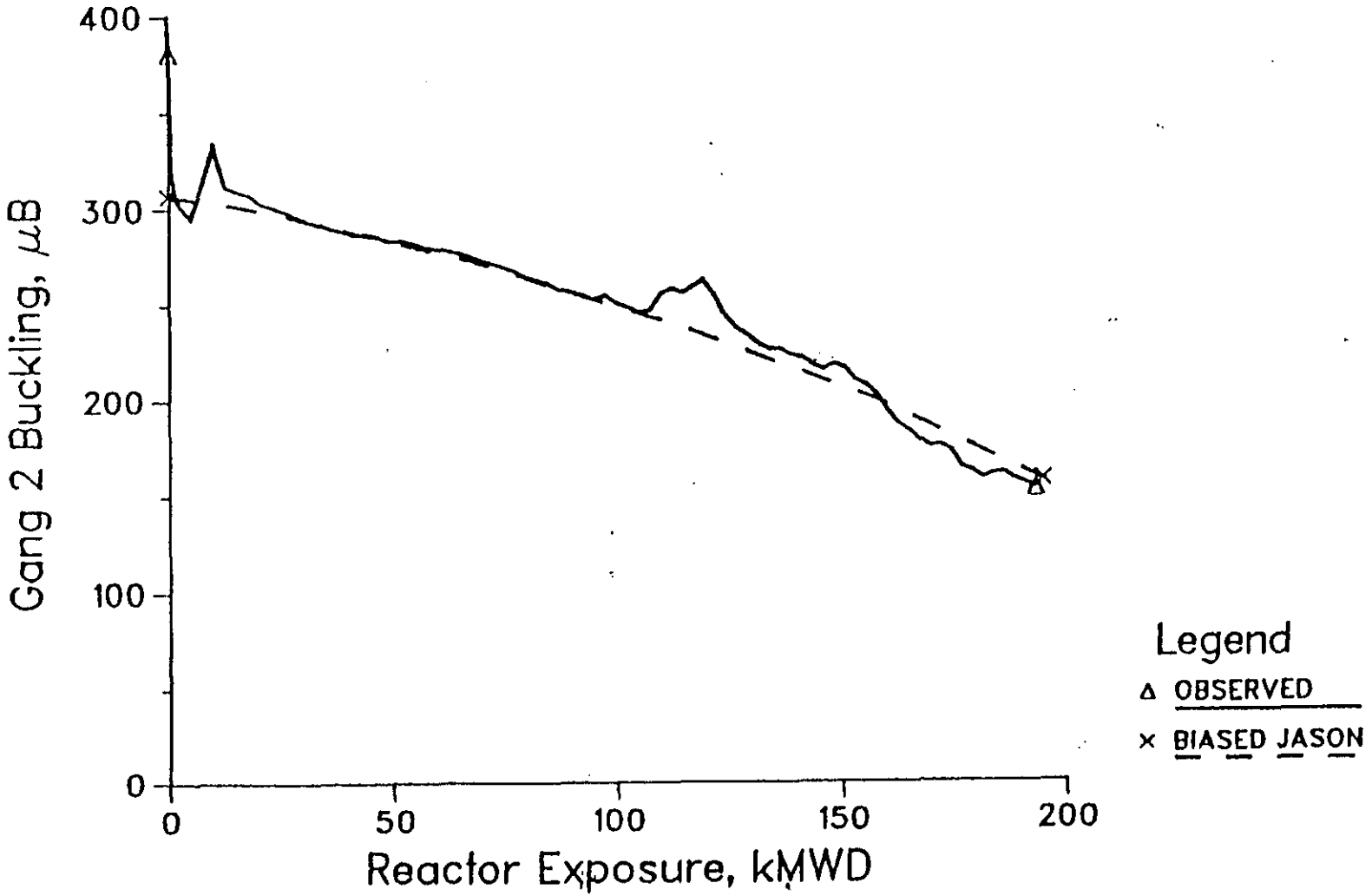

FIGURE B-27

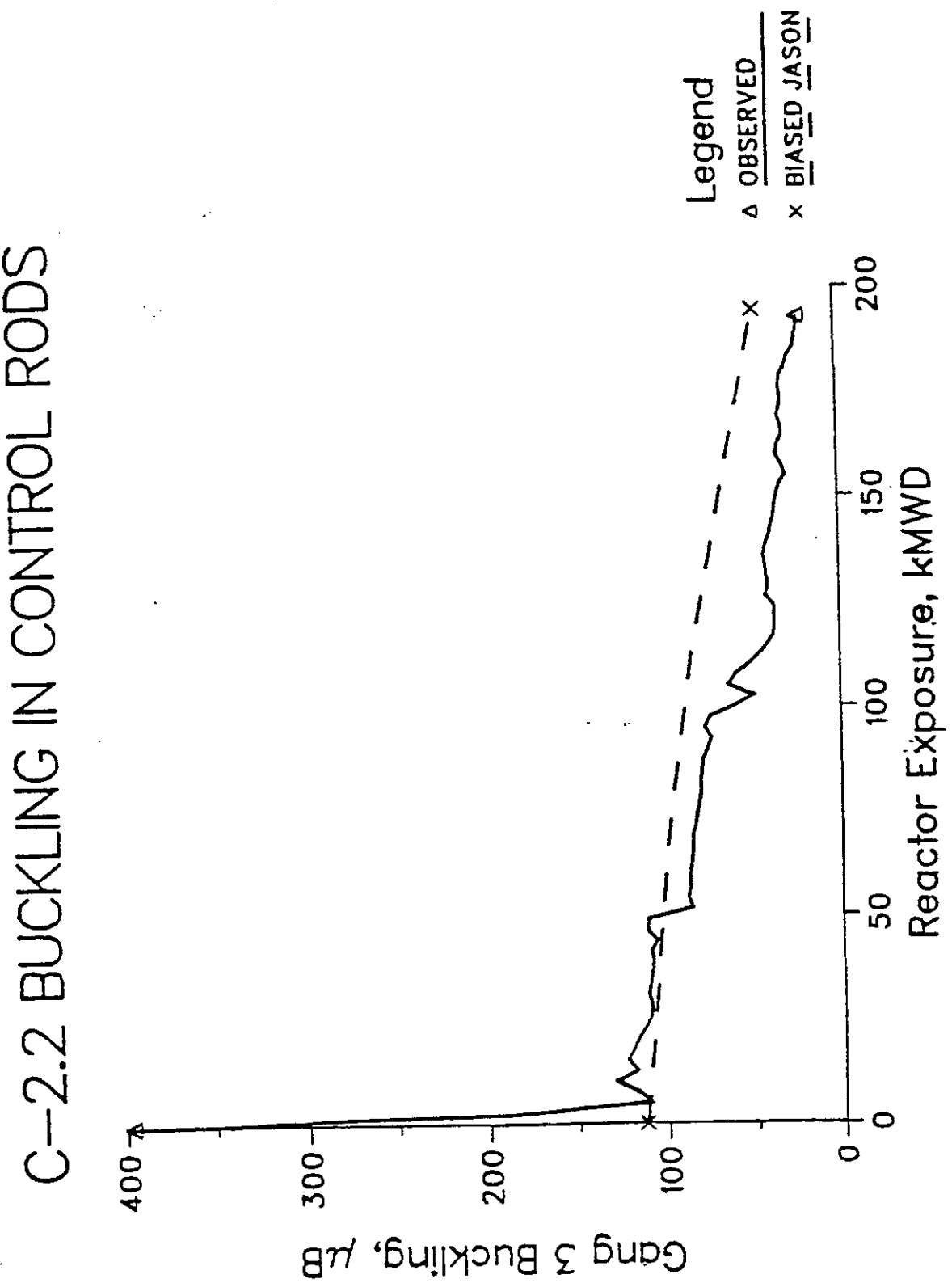
C-2.2 BUCKLING IN CONTROL RODS
Legend
Δ OBSERVED
× BIASED JASON
Gang 3 Buckling, μB
400
300
200
100
0
0
50
100
150
200
Reactor Exposure, kMWD

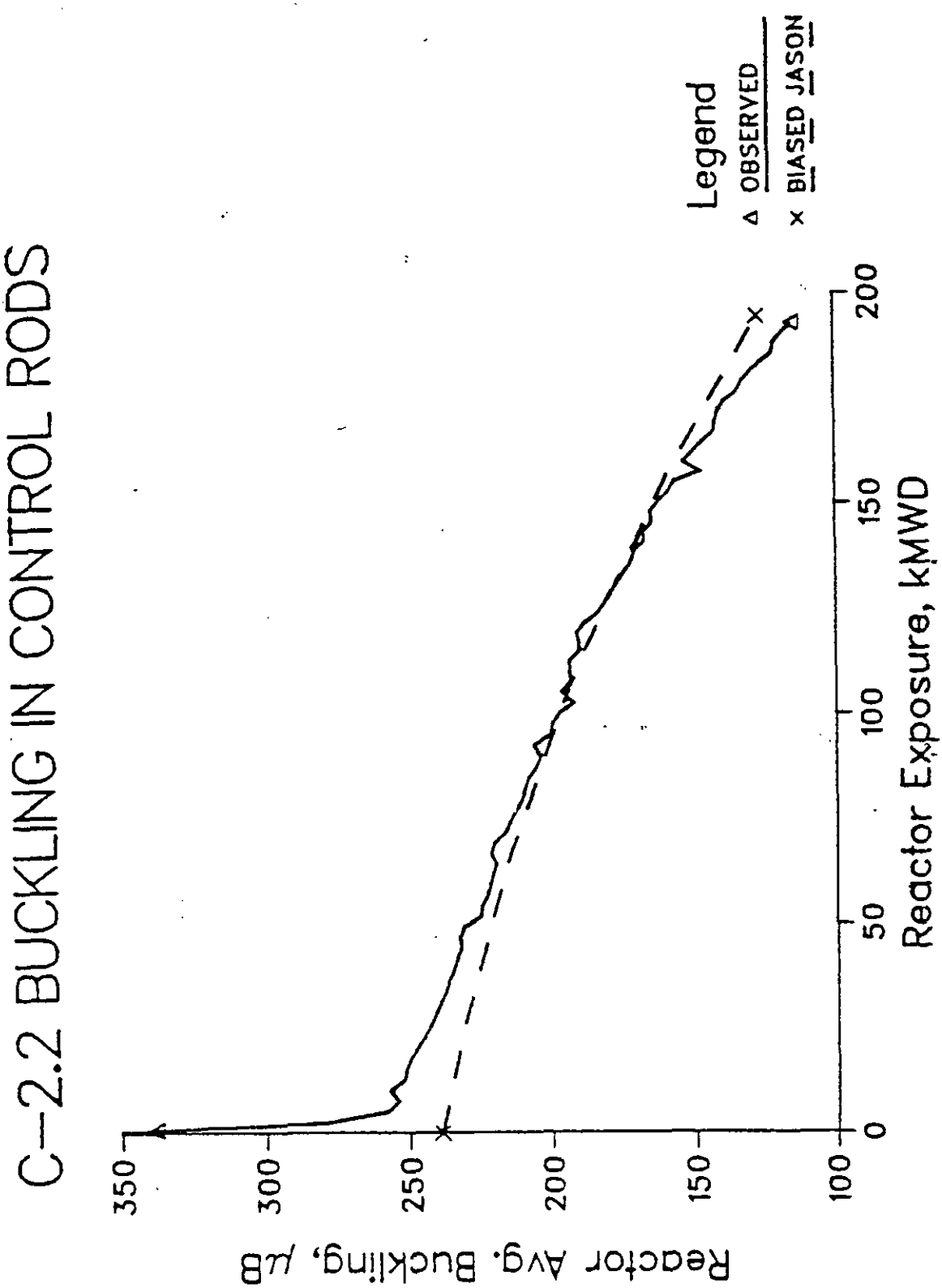
C-2.2 BUCKLING IN CONTROL RODS
Legend
△ OBSERVED
× BIASED JASON
Reactor Avg. Buckling, μB
350
300
250
200
150
100
0
50
100
150
200
Reactor Exposure, kMWD

FIGURE B-28

FIGURE B-29

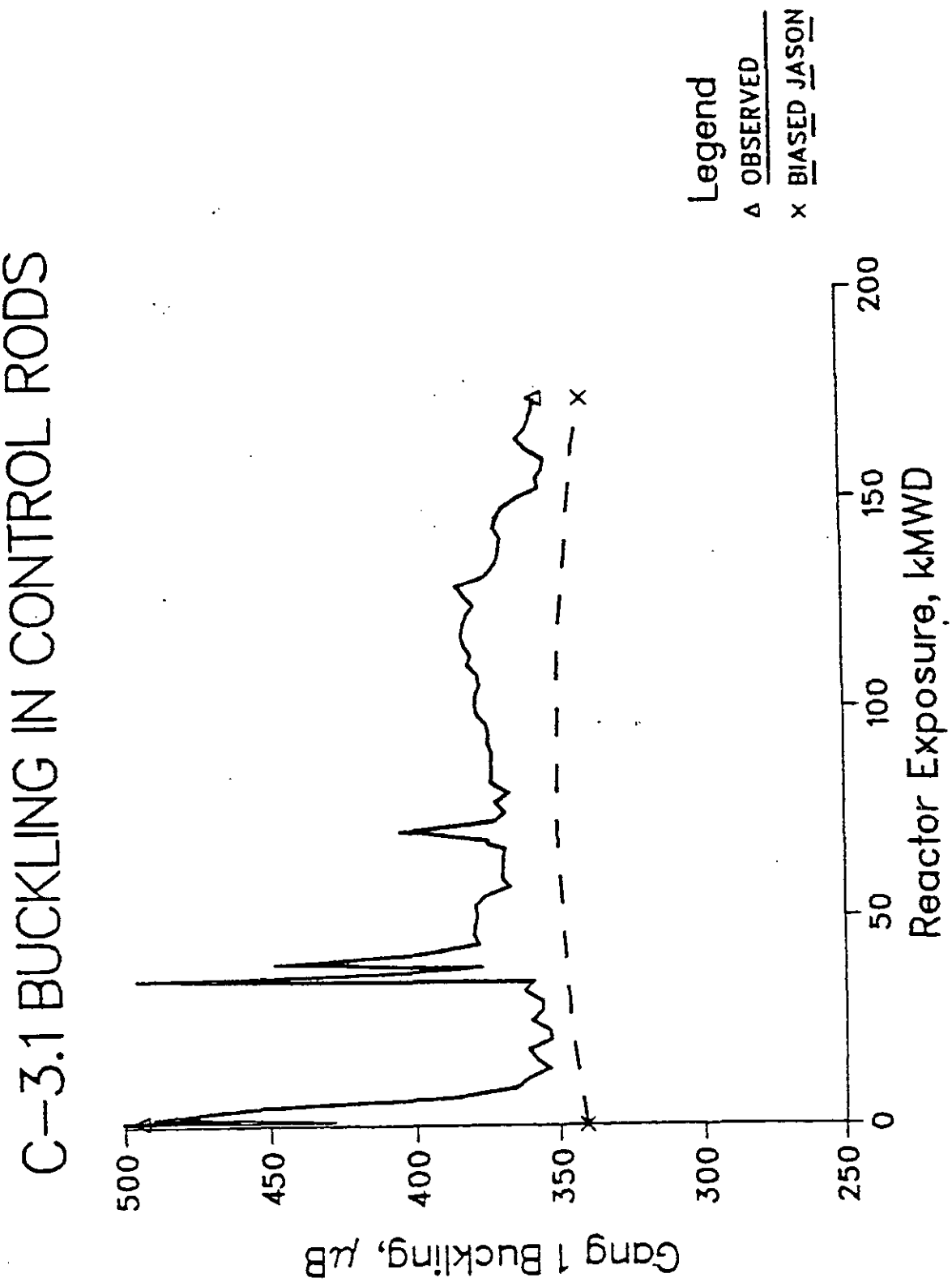
C-3.1 BUCKLING IN CONTROL RODS
Legend
△ OBSERVED
× BIASED JASON
Gang 1 Buckling, μB
500
450
400
350
300
250
0
50
100
150
200
Reactor Exposure, kMWD

FIGURE B-30

C-3.1 BUCKLING IN CONTROL RODS

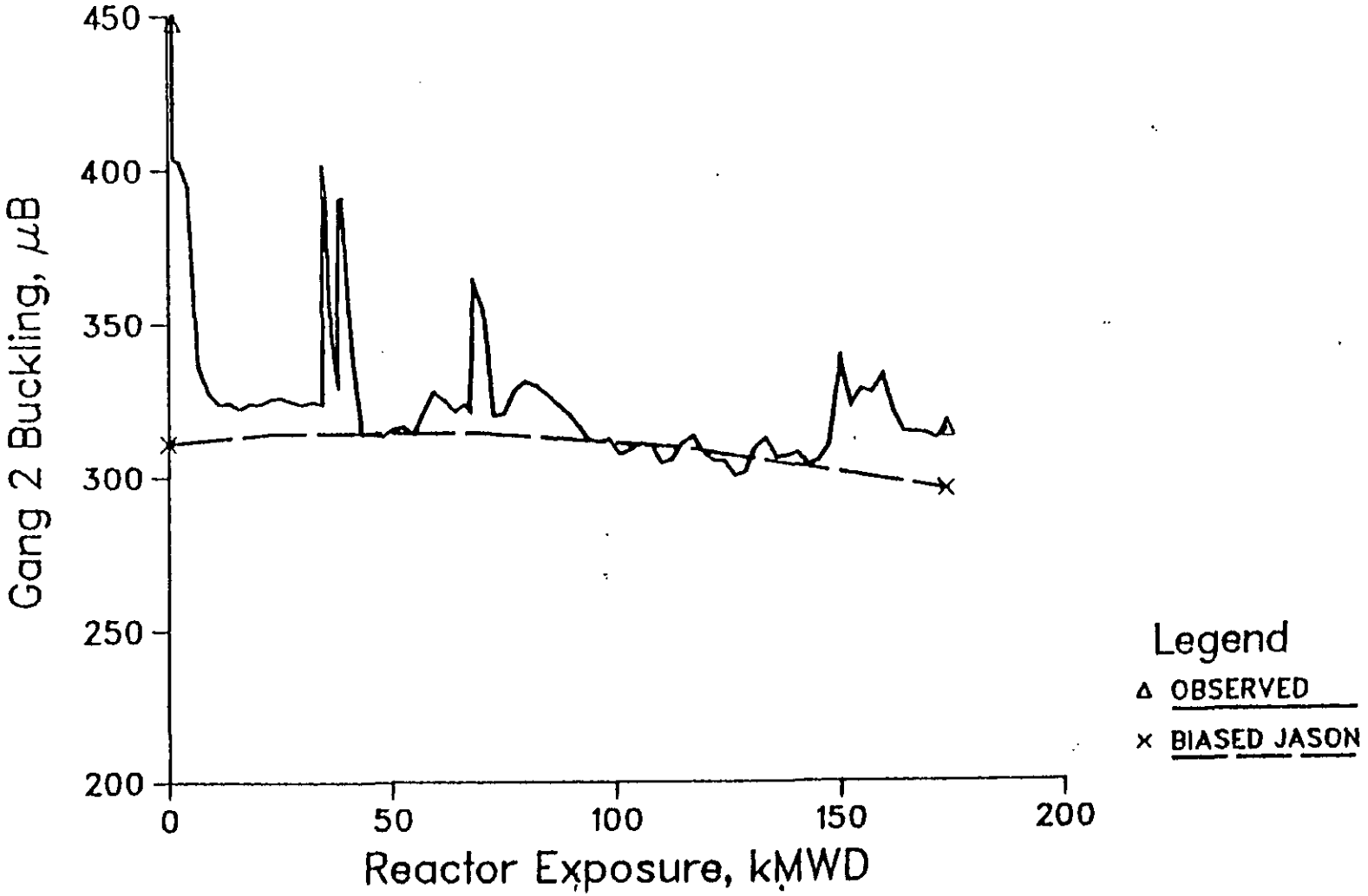

FIGURE B-31

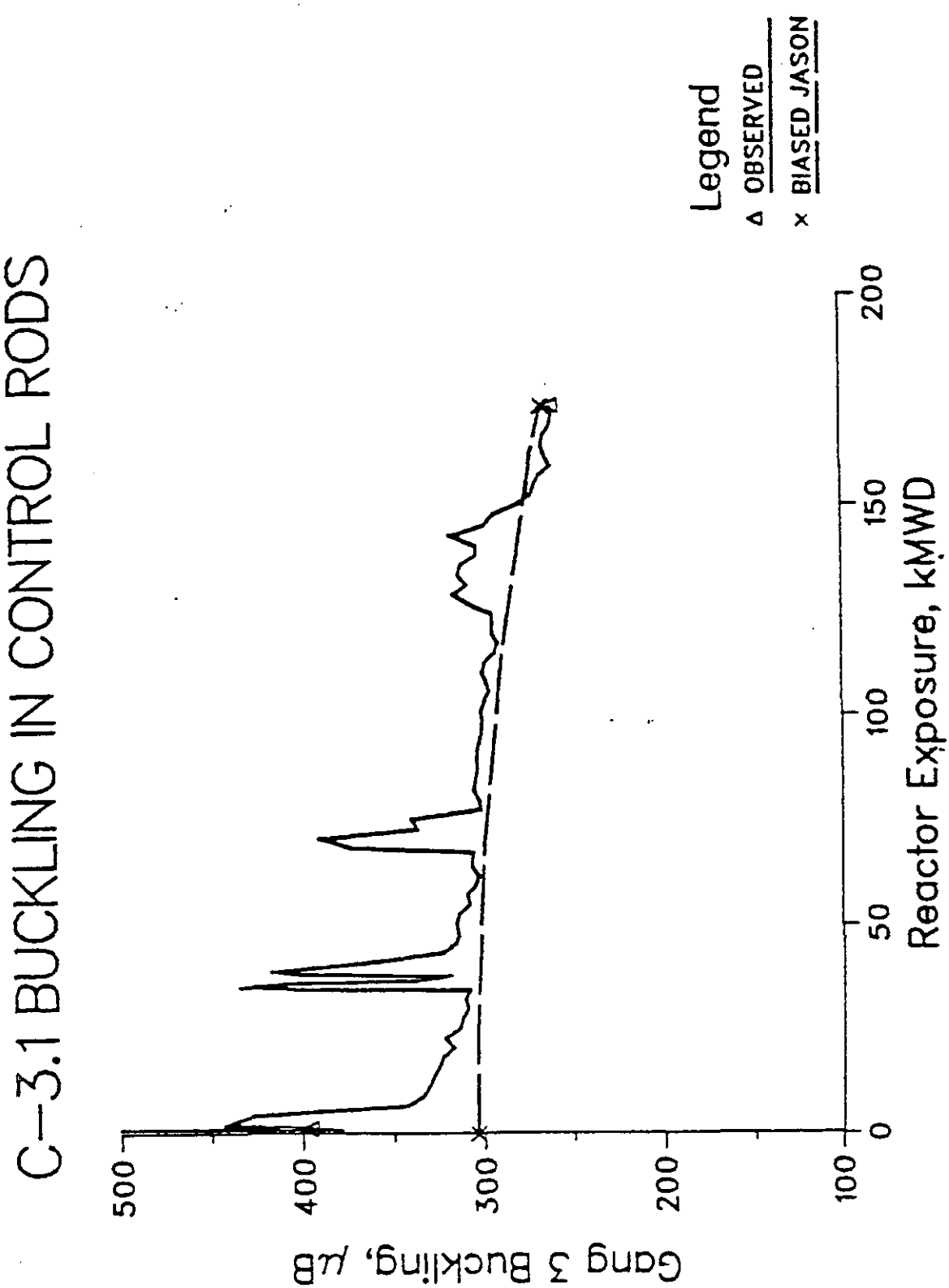
C-3.1 BUCKLING IN CONTROL RODS
Legend
OBSERVED
BIASED JASON
Gang 3 Buckling, μB
500
400
300
200
100
0
50
100
150
200
Reactor Exposure, kMWD

FIGURE B-32

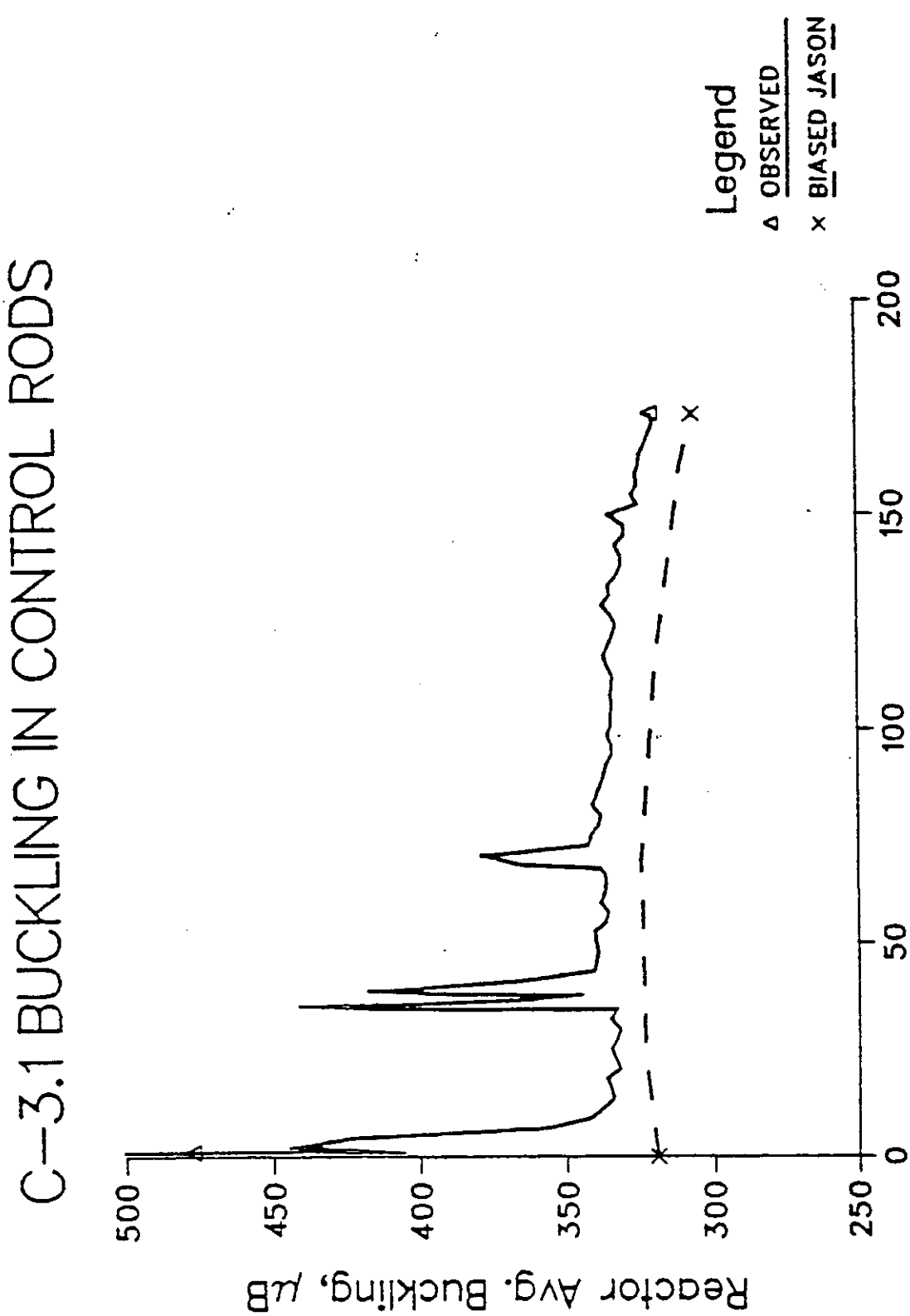
C-3.1 BUCKLING IN CONTROL RODS
Legend
Δ OBSERVED
× BIASED JASON
Reactor Avg. Buckling, μB
500
450
400
350
300
250
0
50
100
150
200
Reactor Exposure, kMWD

FIGURE B-33

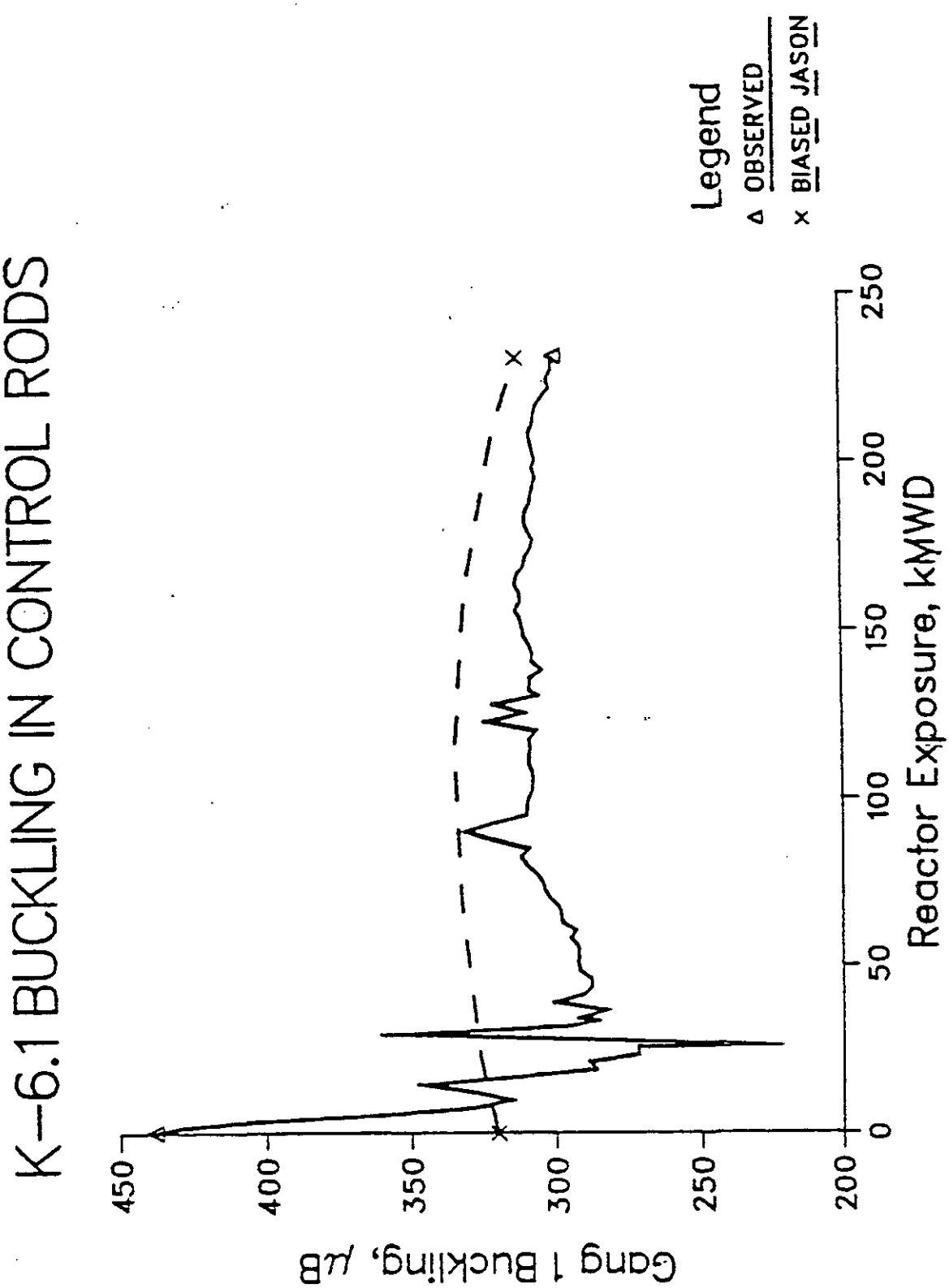
K-6.1 BUCKLING IN CONTROL RODS
Legend
△ OBSERVED
× BIASED JASON
Gang 1 Buckling, πB
450
400
350
300
250
200
0
50
100
150
200
250
Reactor Exposure, kMWD

FIGURE B-34

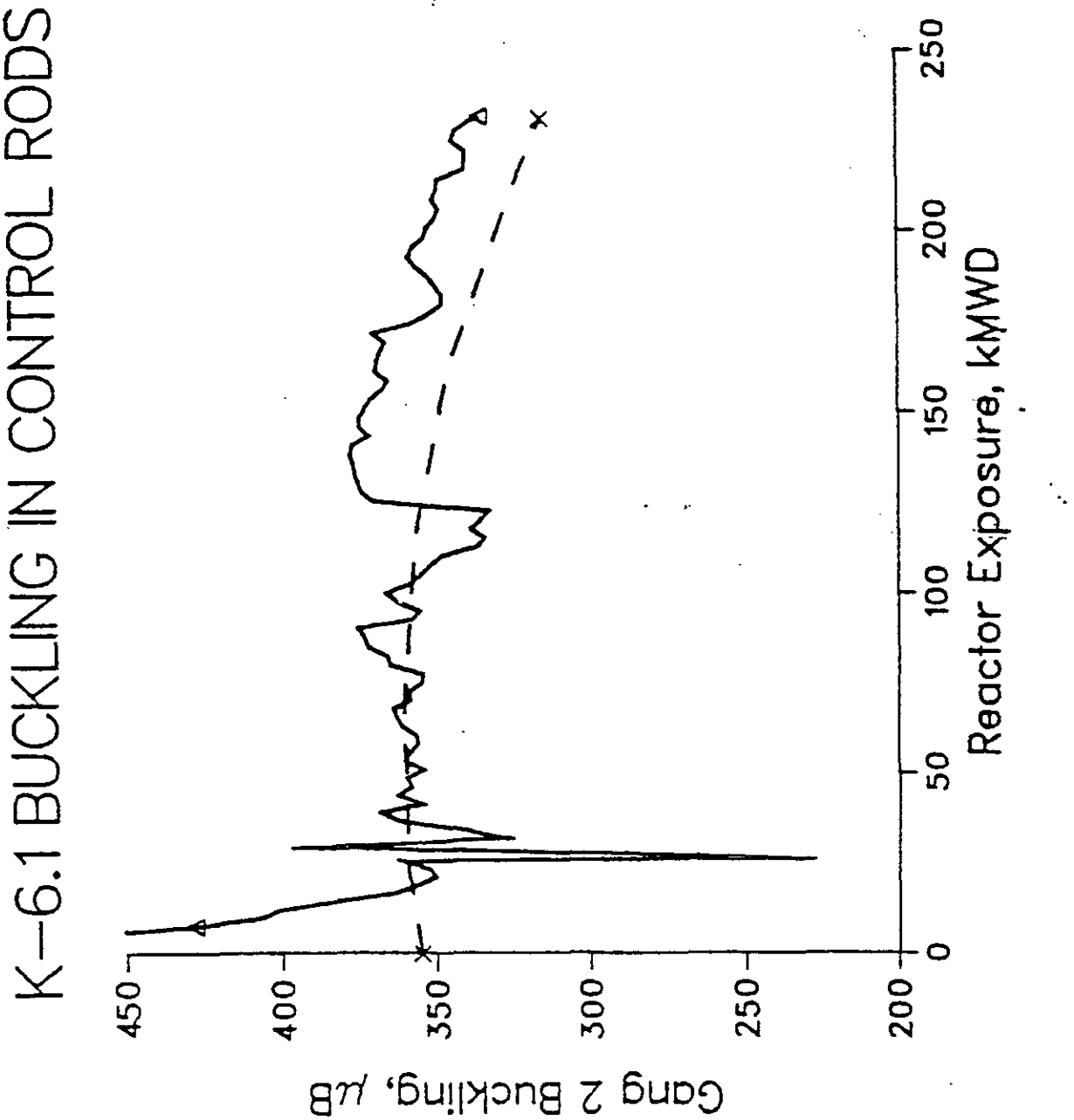
K-6.1 BUCKLING IN CONTROL RODS
Legend
Δ OBSERVED
× BIASED JASON
Gang 2 Buckling, μB
450
400
350
300
250
200
0
50
100
150
200
250
Reactor Exposure, kMWD

FIGURE B-35

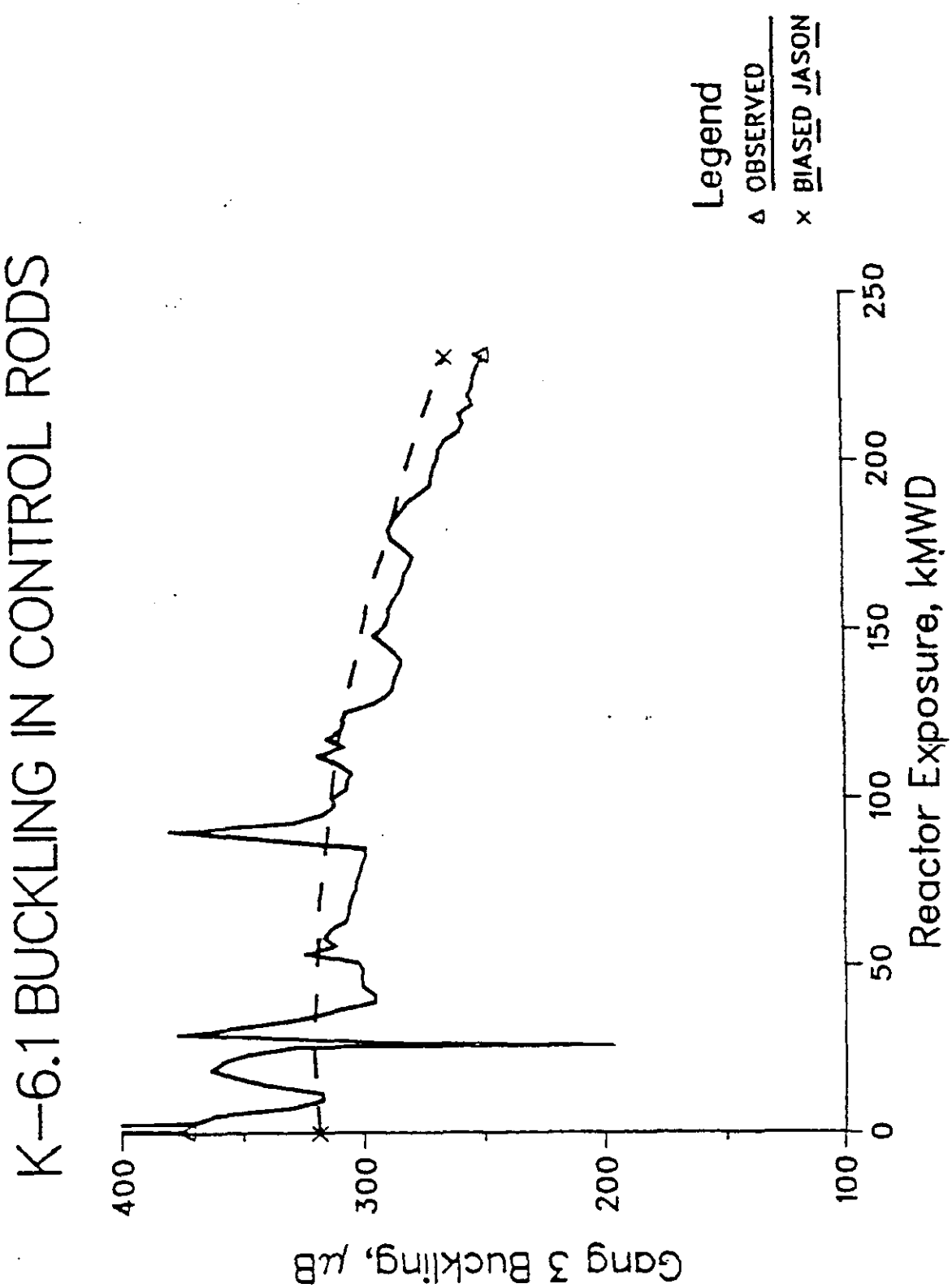
K-6.1 BUCKLING IN CONTROL RODS
Legend
Δ OBSERVED
× BIASED JASON
Gang 3 Buckling, μB
400
300
200
100
0
50
100
150
200
250
Reactor Exposure, kMWD

FIGURE B-36

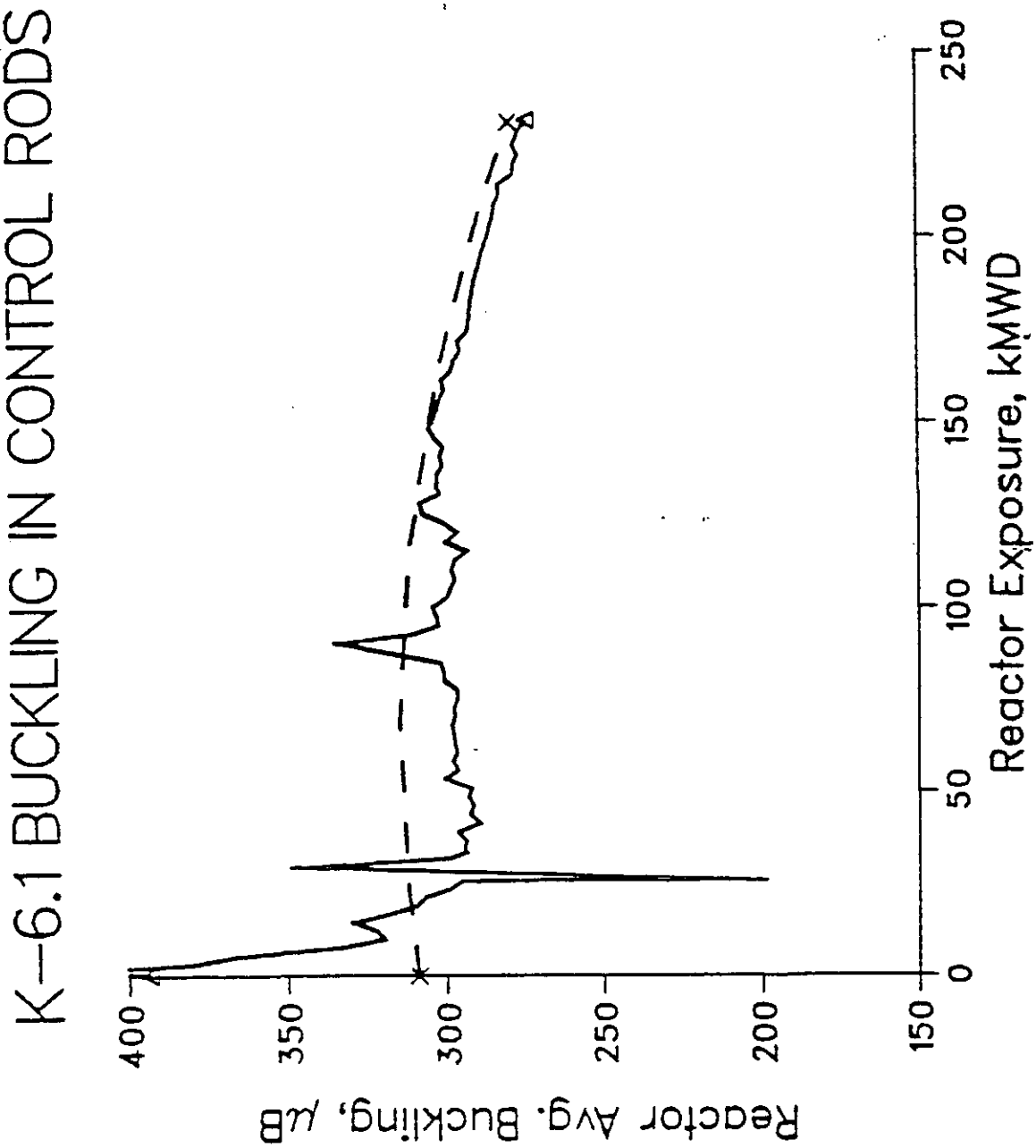
K-6.1 BUCKLING IN CONTROL RODS
Legend
△ OBSERVED
× BIASED JASON
Reactor Avg. Buckling, μB
400
350
300
250
200
150
0
50
100
150
200
250
Reactor Exposure, kMWD

FIGURE B-37

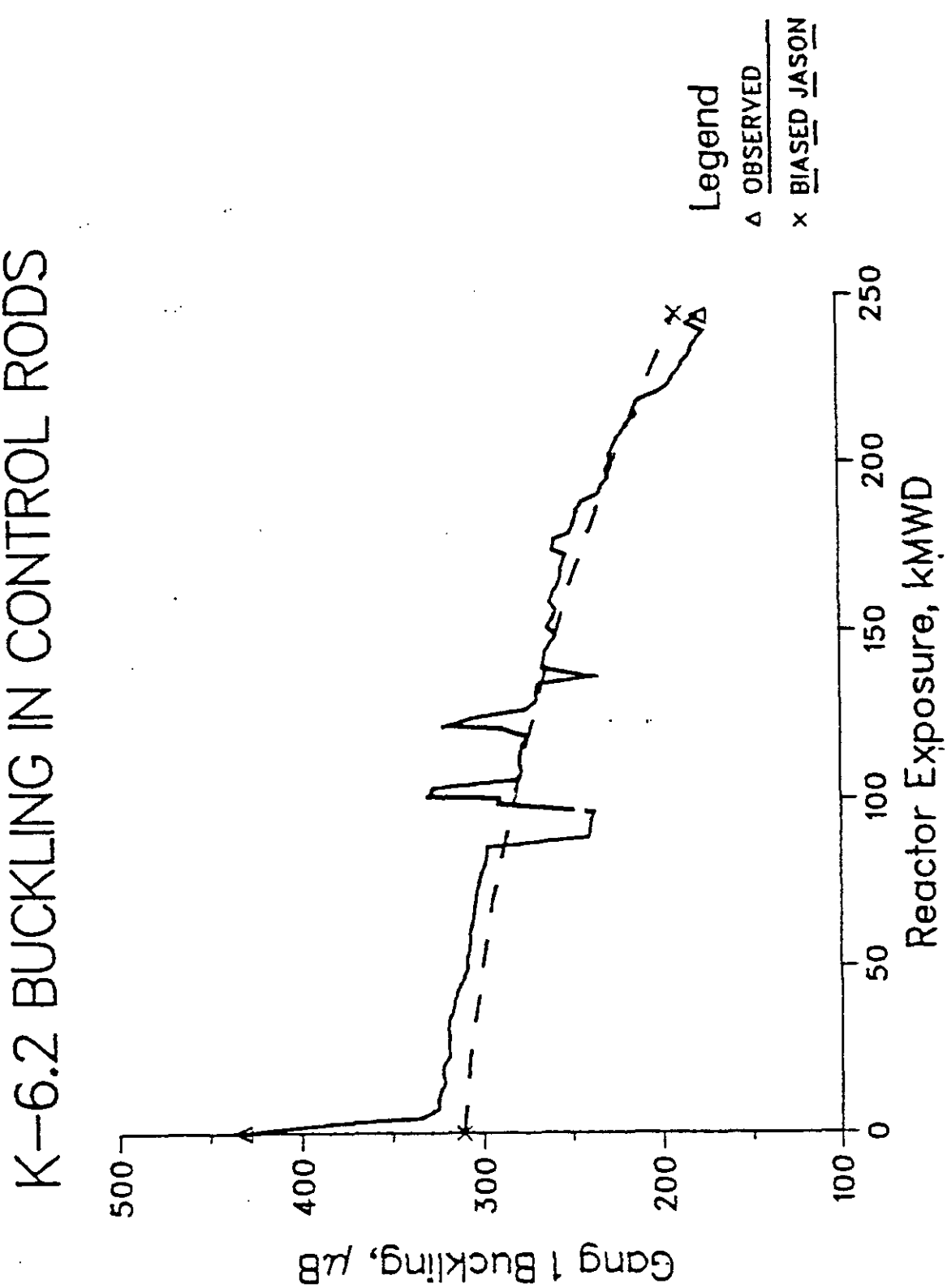
K-6.2 BUCKLING IN CONTROL RODS
Legend
△ OBSERVED
× BIASED JASON
Gang 1 Buckling, μB
500
400
300
200
100
0
50
100
150
200
250
Reactor Exposure, kMWD

FIGURE B-38

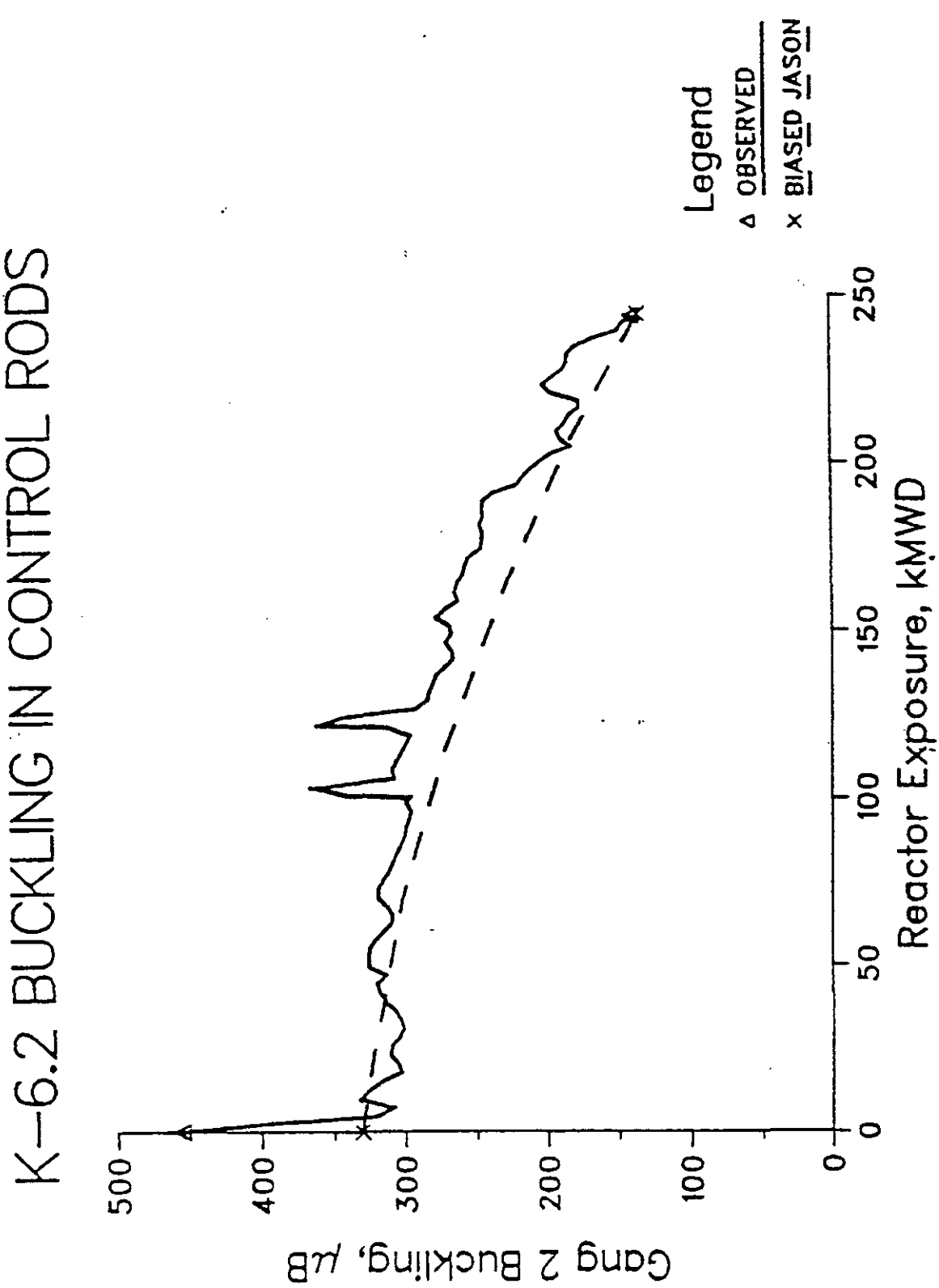
K-6.2 BUCKLING IN CONTROL RODS
Legend
△ OBSERVED
× BIASED JASON
Gang 2 Buckling, μB
500
400
300
200
100
0
0
50
100
150
200
250
Reactor Exposure, kMWD

FIGURE B-39

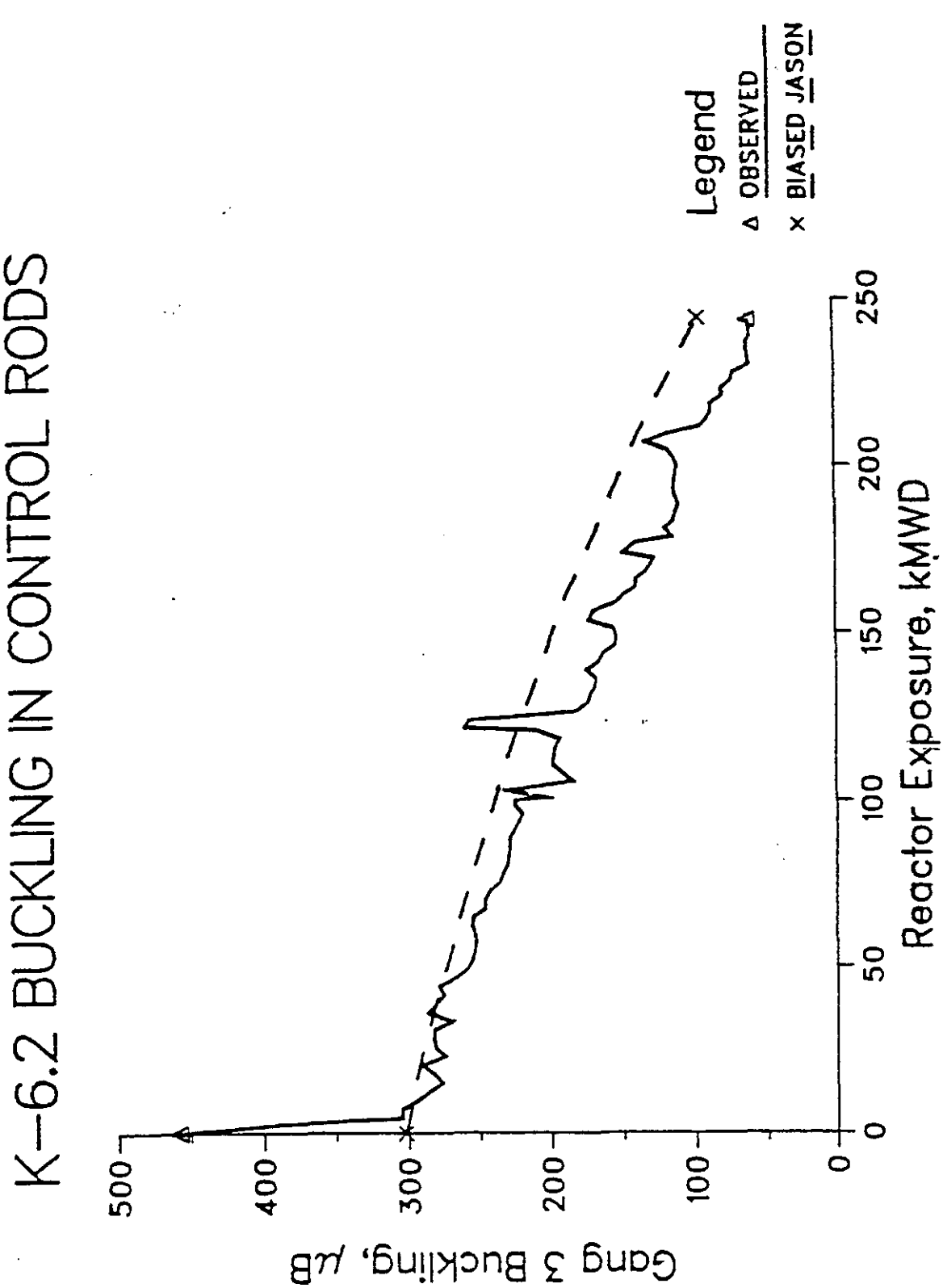
K-6.2 BUCKLING IN CONTROL RODS
Legend
Δ OBSERVED
× BIASED JASON
Gang 3 Buckling, μB
500
400
300
200
100
0
0
50
100
150
200
250
Reactor Exposure, kMWD

FIGURE B-40

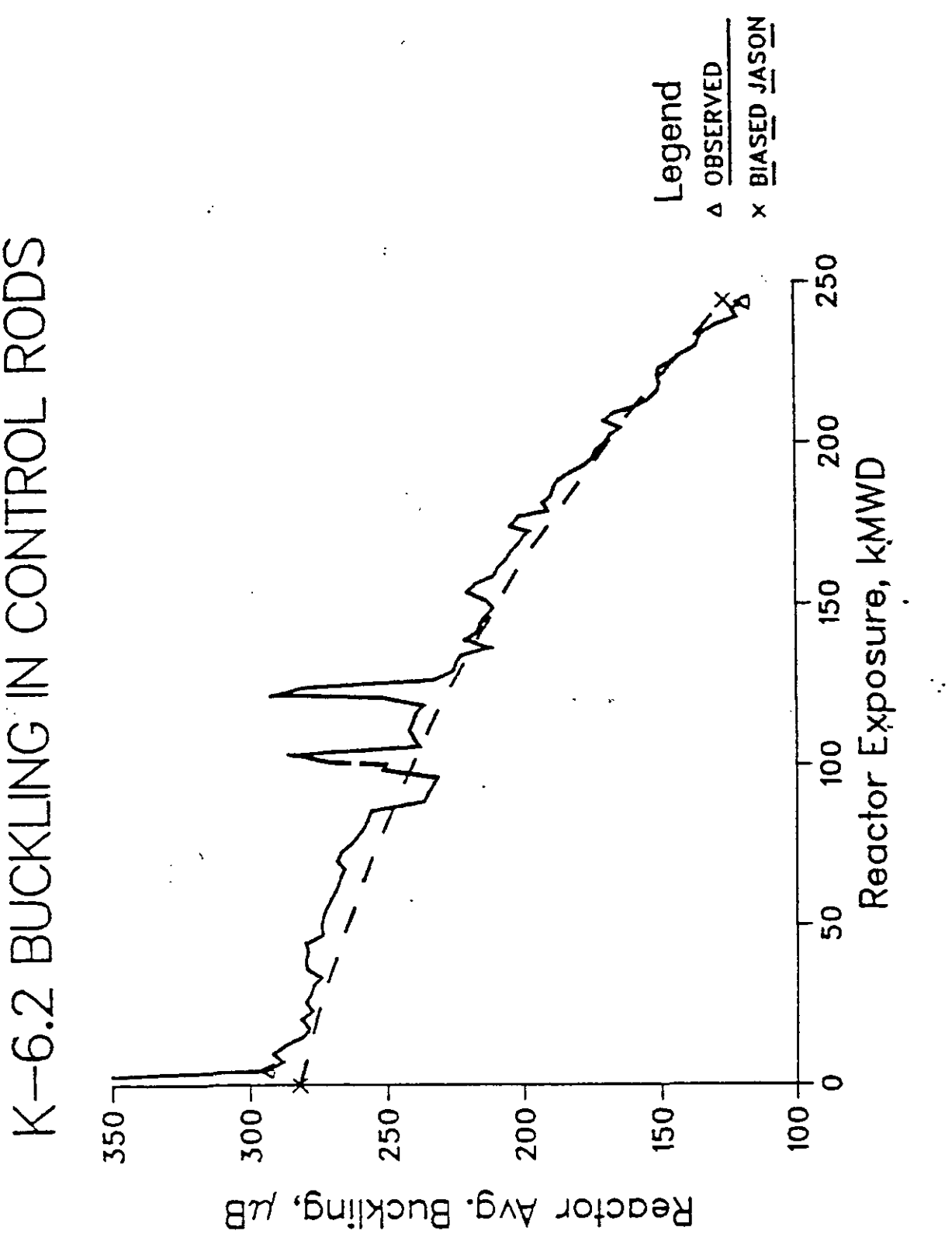
K-6.2 BUCKLING IN CONTROL RODS
Legend
△ OBSERVED
× BIASED JASON
Reactor Avg. Buckling, μB
350
300
250
200
150
100
0
50
100
150
200
250
Reactor Exposure, kMWD